JGR Planets

RESEARCH ARTICLE

10.1029/2024JE008537

Global Transport of Chlorine Species in the Martian Atmosphere and the Resulting Surface Distribution of Perchlorates

K. Rajendran[1], P. M. Streeter[1], S. R. Lewis[1], M. K. D. Duffy[1], J. A. Holmes[1], K. S. Olsen[2], O. Korablev[3], and M. R. Patel[1,4]

[1]School of Physical Sciences, The Open University, Milton Keynes, UK, [2]Department of Physics, University of Oxford, Oxford, UK, [3]Space Research Institute (IKI), Moscow, Russia, [4]Space Science and Technology Department, Science and Technology Facilities Council, Rutherford Appleton Laboratory, Oxfordshire, UK

Abstract Recent observations by instruments aboard the ExoMars Trace Gas Orbiter (TGO) have revealed the seasonal presence of hydrogen chloride (HCl) in the Martian atmosphere. This discovery may have important implications for Martian photochemistry as chlorine species are chemically active, and it may provide a link between the atmosphere and known surface reservoirs of chlorine. However, the global distribution of atmospheric HCl is unknown beyond the very sparse TGO observations, and the source and sink processes driving the observed variability of HCl are not currently understood. We used a Martian global climate model to investigate, for the first time, the spatial distribution of chlorine species in the Martian atmosphere, and the resulting distribution of surface perchlorates formed via adsorption of atmospheric chlorine species. We adapted an existing Martian photochemical scheme to include gas-phase chlorine chemistry with HCl as the source species, and the resulting atmospheric perchloric acid was allowed to deposit onto the Martian surface via a heterogeneous adsorption scheme. We found that odd-oxygen (O, O_3) and odd-hydrogen (H, OH, HO_2) species play a major role in controlling the distribution of atmospheric chorine species. Surface perchlorate deposition was found to occur preferentially at high latitudes; in the tropics, the perchlorate distribution was anti-correlated with surface thermal inertia and agreed qualitatively with observations of surface chlorine. Our model predicted a relative enhancement of HCl in polar regions, but it did not reproduce the observed strong seasonality of HCl, suggesting that heterogeneous chemistry may be required to explain the observed chlorine cycle.

Plain Language Summary Instruments aboard the ExoMars Trace Gas Orbiter have recently measured a seasonal presence of hydrogen chloride in the Martian atmosphere. This finding is surprising as an active chlorine cycle was not thought to be present on Mars, and it is not currently known what the processes driving this cycle are. Chlorine has also been found on the Martian surface as perchlorate, which is hazardous for life but is also a potential fuel source. The presence of atmospheric chlorine thus raises the possibility of a link between the surface and atmospheric chlorine reservoirs. In this work, we adapted a Martian global climate model to investigate the chemistry and three-dimensional transport of chlorine species in the Martian atmosphere, as well as where these species might accumulate on the surface. We found that odd-oxygen and odd-hydrogen species play a major role in influencing the spatial and seasonal distributions of the chlorine species. The surface distribution of perchlorate in our model is in qualitative agreement with several (but not all) features of the surface chlorine distribution observed by satellites. Our model did not reproduce the observed large seasonal variation of atmospheric hydrogen chloride, however, and we suggest potential mechanisms that might explain this.

Key Points:

- Known gas-phase chemistry predicts elevated atmospheric hydrogen chloride in Martian polar regions, but cannot reproduce its seasonality
- Modeled adsorption of atmospherically generated perchloric acid onto the Martian surface occurs preferentially at high latitudes
- The tropical perchlorate distribution is anti-correlated with surface thermal inertia and is consistent with Gamma Ray Spectrometer data

Supporting Information:

Supporting Information may be found in the online version of this article.

Correspondence to:

K. Rajendran,
kylash.rajendran@open.ac.uk

Citation:

Rajendran, K., Streeter, P. M., Lewis, S. R., Duffy, M. K. D., Holmes, J. A., Olsen, K. S., et al. (2025). Global transport of chlorine species in the Martian atmosphere and the resulting surface distribution of perchlorates. *Journal of Geophysical Research: Planets*, *130*, e2024JE008537. https://doi.org/10.1029/2024JE008537

Received 29 JUN 2024
Accepted 23 DEC 2024

1. Introduction

Atmospheric hydrogen chloride (HCl) has recently been detected in the Martian atmosphere by instruments aboard the ExoMars Trace Gas Orbiter (TGO), first with the Atmospheric Chemistry Suite (Korablev et al., 2021; Olsen, Trokhimovskiy, et al., 2021) and later confirmed with the Nadir and Occultation for MArs Discovery (Aoki et al., 2021) spectrometers. Prior to the TGO detections, Earth-based attempts to find chlorine species had only established upper detection limits (e.g., Hartogh et al., 2010; Villanueva et al., 2013) and had implied an absence of contemporary chlorine-based chemistry in the Martian atmosphere. These measurements were only performed during the cold aphelion season, however, and a recent Earth-based measurement campaign following the TGO discoveries has since detected HCl in the perihelion season (Aoki et al., 2024).

The TGO orbital HCl measurements have revealed a seasonal cycle in the observed HCl, with HCl mixing ratios rising rapidly in both hemispheres during the perihelion (dusty) season (areocentric solar longitude, L_S = 180–360°), while remaining low in the clearer aphelion season apart from a small number of detections (Aoki et al., 2021; Olsen, Trokhimovskiy, et al., 2021). The source and sink processes driving the distinct seasonal variability of HCl have not yet been determined and are the subjects of ongoing research. It has been suggested that mineral dust may be the source of the observed HCl (Aoki et al., 2021; Korablev et al., 2021; Olsen, Trokhimovskiy, et al., 2021), possibly via heterogeneous interactions between chloride-bearing dust aerosols and atmospheric hydrogen radicals (Krasnopolsky, 2022). The rapid loss of HCl after the dusty season has been linked to the uptake of HCl on water ice aerosols, a mechanism consistent with an observed anti-correlation between HCl and water ice in the lower atmosphere (Luginin et al., 2024; Olsen et al., 2024a, 2024b).

Prior to the detection of HCl in the Martian atmosphere, perchlorates and chloride-bearing minerals had been identified on the Martian surface by in situ measurements. These include measurements of perchlorate salts by the Phoenix lander (Hecht et al., 2009) and of chlorinated hydrocarbons and perchlorates by the Curiosity rover (Glavin et al., 2013). From orbit, the distributions of surface chlorine and chloride-bearing minerals have been mapped by the Gamma Ray Spectrometer (GRS) (Keller et al., 2006) and Thermal Emission Imaging System (THEMIS) (Osterloo et al., 2008) aboard the Mars Odyssey spacecraft, as well as by the Compact Reconnaissance Imaging Spectrometer for Mars (Murchie et al., 2009) aboard the Mars Reconnaissance Orbiter and the "Observatoire pour la Minéralogie, l'Eau, les Glaces et l'Activité" (OMEGA) spectrometer aboard Mars Express (Ruesch et al., 2012).

A number of mechanisms have been proposed to explain the presence of perchlorates on the Martian surface. Catling et al. (2010) hypothesized that gas-phase atmospheric oxidation of chlorine volatiles could explain the observed perchlorate salts both on Mars and in the Atacama desert on Earth. However, Smith et al. (2014) used a one-dimensional (1D) atmospheric column model to conclude that perchlorate formation purely via gas-phase oxidation of volcanic chlorine was insufficient to explain the Phoenix measurements, and that non-gas-phase processes (such as heterogeneous reactions) were likely an important factor. Wilson et al. (2016) suggested that radiolysis of the Martian surface by galactic cosmic rays could provide an efficient pathway for chlorine oxidation and explain observed surface measurements. Wu et al. (2018) proposed multi-phase redox plasma chemistry from electrostatic activity by analyzing laboratory experiments under Martian conditions. They suggested Cl-bearing surface minerals and atmospheric free radicals may react together to produce surface perchlorates. Whilst there have been no direct observations of electrical discharges within the Martian atmosphere, these have been inferred indirectly by Ruf et al. (2009). Finally, Edgar et al. (2022) have recently demonstrated in laboratory experiments that perchlorates can be formed through the mechanical activation of silicate rocks in the presence of halite salts.

The detection of HCl in the Martian atmosphere provides an impetus to revisit the work of Catling et al. (2010) and Smith et al. (2014), who invoked HCl as the source species for perchlorate formation via an atmospheric pathway. As both of these prior studies only modeled atmospheric chlorine chemistry in a single column, no study has yet investigated the spatial distribution of chemical production and loss of chlorine species, or the impacts of atmospheric dynamics and transport processes on their spatial distributions. Therefore, in this study we use a Mars Global Climate Model (MGCM) incorporating gas-phase chlorine chemistry to investigate, for the first time, the impacts of global transport on the distribution of chlorine species in the Martian atmosphere. We then use our model to characterize the distribution of surface perchlorates arising from the adsorption of atmospheric perchloric acid onto the Martian surface.

Our focus in this study is on the relationship between gas-phase chemistry and transport processes, which will aid in our understanding of the non-heterogeneous processes affecting chlorine species and provide a benchmark for future work. Given the potential importance of factors such as gas-phase chlorine chemistry, heterogeneous chemistry on aerosol surfaces, and transport processes (Olsen, Trokhimovskiy, et al., 2021; Taysum et al., 2024) in understanding the seasonal, vertical, and spatial distribution of observed atmospheric HCl, it is important to understand how these separate elements affect the global chlorine distribution on their own, and subsequently how they combine. In a companion work (P. M. Streeter et al., 2025) we will focus on the impact of the inclusion of heterogeneous chemical processes on chlorine chemistry using the same MGCM.

In Section 2 we introduce the MGCM used and describe the implementation of the chlorine chemistry scheme. The gas-phase chemical pathways and distributions of the chlorine species contributing to perchlorate formation

are discussed in Section 3, and the resulting surface distribution of perchlorate is presented in Section 4. We discuss our findings in Section 5.

2. The Mars Global Climate Model

We model the Martian atmosphere with the MGCM used at the Open University (UK), which is the spectral variant of the Mars Planetary Climate Model (Forget et al., 1999, 2022). This model utilizes a spectral dynamical solver (Hoskins & Simmons, 1975) which represents horizontal atmospheric fields as a weighted sum of spherical harmonic functions, thereby improving representation of waves and dynamical fields near the poles. Vertical discretization is achieved using a finite difference scheme that conserves both energy and angular momentum (Simmons & Burridge, 1981). The dynamical core is coupled to a semi-Lagrangian tracer advection scheme (Newman et al., 2002) and a set of Martian physics routines. These include schemes for radiative transfer, CO_2 condensation and sublimation, photochemistry, dust processes, boundary layer processes and cloud microphysics (Colaïtis et al., 2013; Forget et al., 1999; Lefèvre et al., 2004; Madeleine et al., 2011; Navarro et al., 2014). The model incorporates a data assimilation scheme (S. Lewis & Barker, 2005; Lorenc et al., 1991) that has been used extensively for investigations of the Martian atmosphere. Recent work using this model includes investigations of the water cycle and supersaturation during a global dust storm year (Holmes et al., 2022), multi-year variations to the northern polar vortex (P. Streeter et al., 2023) including during an equinoctial dust storm (P. Streeter et al., 2021), and atmospheric super-rotation (Rajendran et al., 2021).

2.1. Chlorine Scheme

In order to study chlorine chemistry in the Martian atmosphere, we extended the existing model photochemistry scheme of Lefèvre et al. (2004) to incorporate 11 new chlorine species: hydrogen chloride (HCl), atomic chlorine (Cl), molecular chlorine (Cl_2), chlorine monoxide (ClO), hydrogen hypochlorite (HOCl), chlorine peroxy (ClOO), chlorine dioxide (OClO), dichlorine dioxide (Cl_2O_2), chlorine trioxide (ClO_3), chlorine perchlorate (Cl_2O_4) and perchloric acid ($HClO_4$). The chlorine scheme was adapted from the photochemical model presented in Catling et al. (2010), which was designed to use hydrogen chloride as the sole source of chlorine, resulting in the production of perchloric acid as the final product.

Tables 1 and 2 list the full set of gas-phase and photolysis reactions that were included in the photochemistry module for the purposes of this study. Reaction rates were updated using the most recent version of the JPL atmospheric chemistry evaluation (Burkholder et al., 2019). In order to account for the higher efficiency of CO_2 as a third body compared to N_2, all the new 3-body reactions were multiplied by a factor of 2.5 (Lefèvre et al., 2004). For the new photolysis reactions, the actinic flux calculations were performed using a version of the Tropospheric Ultraviolet (TUV) model (Madronich & Flocke, 1999) that had been adapted for Mars (Lefèvre et al., 2004). The actinic flux was first calculated offline in a lookup table for a range of values of temperature, solar zenith angle, ozone column density, atmospheric column density, dust opacity, and Sun-Mars distance; during the model run, photolysis rates were calculated by interpolating across the lookup table.

Some of the reaction rates in Table 1 are uncertain. In particular, the formation of ClO_3 (`x012`) and its reaction with OH (`x030`) are key steps in the formation of $HClO_4$, but the relevant reaction rates have yet to be determined experimentally. Simonaitis and Heicklen (1975) estimated the reaction rates using a combination of old laboratory data and guesses based on analogous reactions. In their one-dimensional modeling study, Catling et al. (2010) reduced the reaction rate estimates of Simonaitis and Heicklen (1975) by a factor of 30 and managed to simulate a reasonable match to observed terrestrial profiles of HCl, Cl, ClO and other chlorine-bearing species. The same tuned reaction rates were used by Smith et al. (2014) in their follow-up study of perchlorate formation in the Martian atmosphere, and therefore we use these reaction rates in our study as well. Changes to the reaction rate would affect the total amount of atmospheric perchloric acid produced in our model, but are not expected to significantly affect the resulting surface distribution of perchlorate as we expect that perchloric acid will remain well-mixed in the atmosphere.

The photochemical scheme uses the Semi-Implicit Backwards Euler Method (SIBEM; Shimazaki (1985)) to calculate the rate of chemical change of long-lived species. The scheme was applied iteratively in order to conserve mass, and a short chemical timestep of 30 s was used in order to maintain stability of the scheme. At each output timestep, the amount of chlorine in each model grid box was scaled to ensure that the total mass of chlorine in the model remained constant. In order to account for variations in the photochemical lifetimes of different

Table 1
The Gas-Phase Chemical Reactions, Including New Reactions Involving Chlorine Species, That Were Included in the Mars Global Climate Model Photochemistry Module for This Study

ID	Reaction	Rate coefficient	Reference
a_{001}	$O + O_2 \xrightarrow{M} O_3$	$2.075 \times 6.0 \times 10^{-34}\left(\frac{T}{300}\right)^{-2.4}[M]$	Burkholder et al. (2019)
a_{002}	$O + O \xrightarrow{M} O_2$	$2.365 \times 10^{-33} e^{485/T}[M]$	Campbell and Gray (1973)
a_{003}	$O + O_3 \rightarrow O_2 + O_2$	$8.0 \times 10^{-12} e^{-2060/T}$	Burkholder et al. (2019)
b_{001}	$O(^1D) \xrightarrow{M} O$	$7.5 \times 10^{-11} e^{115/T}$	Burkholder et al. (2019)
b_{002}	$O(^1D) + H_2O \rightarrow 2OH$	$1.63 \times 10^{-10} e^{60/T}$	Burkholder et al. (2019)
b_{003}	$O(^1D) + H_2 \rightarrow OH + H$	1.2×10^{-10}	Burkholder et al. (2019)
b_{004}	$O(^1D) + O_2 \rightarrow O + O_2$	$3.3 \times 10^{-11} e^{55/T}$	Burkholder et al. (2019)
b_{005}	$O(^1D) + O_3 \rightarrow 2O_2$	1.2×10^{-10}	Burkholder et al. (2019)
b_{006}	$O(^1D) + O_3 \rightarrow O_2 + 2O$	1.2×10^{-10}	Burkholder et al. (2019)
c_{001}	$O + HO_2 \rightarrow OH + O_2$	$3.0 \times 10^{-11} e^{200/T}$	Burkholder et al. (2019)
c_{002}	$O + OH \rightarrow O_2 + H$	$1.8 \times 10^{-11} e^{180/T}$	Burkholder et al. (2019)
c_{003}	$H + O_3 \rightarrow OH + O_2$	$1.4 \times 10^{-10} e^{-470/T}$	Burkholder et al. (2019)
c_{004}	$H + HO_2 \rightarrow OH + OH$	7.2×10^{-11}	Burkholder et al. (2019)
c_{005}	$H + HO_2 \rightarrow H_2 + O_2$	6.9×10^{-12}	Burkholder et al. (2019)
c_{006}	$H + HO_2 \rightarrow H_2O + O$	1.6×10^{-12}	Burkholder et al. (2019)
c_{007}	$OH + HO_2 \rightarrow H_2O + O_2$	$4.8 \times 10^{-11} e^{250/T}$	Burkholder et al. (2019)
c_{008}	$HO_2 + HO_2 \rightarrow H_2O_2 + O_2$	$3.0 \times 10^{-13} e^{460/T}$	Burkholder et al. (2019)
c_{009}	$OH + H_2O_2 \rightarrow H_2O + HO_2$	1.8×10^{-12}	Burkholder et al. (2019)
c_{010}	$OH + H_2 \rightarrow H_2O + H$	$2.8 \times 10^{-12} e^{-1800/T}$	Burkholder et al. (2019)
c_{011}	$H + O_2 \xrightarrow{M} HO_2$	$k_0 = 2.5 \times 5.3 \times 10^{-32}\left(\frac{T}{300}\right)^{-1.8}$, $k_\infty = 9.5 \times 10^{-11}\left(\frac{T}{300}\right)^{0.4}$	Burkholder et al. (2019)
c_{012}	$O + H_2O_2 \rightarrow OH + HO_2$	$1.4 \times 10^{-12} e^{-2000/T}$	Burkholder et al. (2019)
c_{013}	$OH + OH \rightarrow H_2O + O$	1.8×10^{-12}	Burkholder et al. (2019)
c_{014}	$OH + O_3 \rightarrow HO_2 + O_2$	$1.7 \times 10^{-12} e^{-940/T}$	Burkholder et al. (2019)
c_{015}	$HO_2 + O_3 \rightarrow OH + 2O_2$	$1.0 \times 10^{-14} e^{-490/T}$	Burkholder et al. (2019)
c_{016}	$HO_2 + HO_2 \xrightarrow{M} H_2O_2 + O_2$	$2.5 \times 2.1 \times 10^{-33} e^{920/T}[M]$	Burkholder et al. (2019)
c_{017}	$OH + OH \xrightarrow{M} H_2O_2$	$k_0 = 2.5 \times 6.9 \times 10^{-31}\left(\frac{T}{300}\right)^{-1.0}$, $k_\infty = 2.6 \times 10^{-11}$	Burkholder et al. (2019)
c_{018}	$H + H \xrightarrow{M} H_2$	$2.5 \times 1.8 \times 10^{-30}(T)^{-1.0}[M]$	Baulch et al. (2005)
e_{001}	$OH + CO \rightarrow CO_2 + H$	$1.6 \times 10^{-13} + 3.5 \times 10^{-33}[M]$	Burkholder et al. (2019)
e_{002}	$O + CO \xrightarrow{M} CO_2$	$6.5 \times 10^{-33} e^{-2184/T}[M]$	Burkholder et al. (2019)
x_{001}	$HCl + O \rightarrow OH + Cl$	$1.0 \times 10^{-11} e^{-3300/T}$	Burkholder et al. (2019)
x_{002}	$HCl + OH \rightarrow Cl + H_2O$	$1.8 \times 10^{-12} e^{-250/T}$	Burkholder et al. (2019)
x_{003}	$HCl + O(1D) \rightarrow HCl + O$	1.8×10^{-11}	Burkholder et al. (2019)
x_{004}	$HCl + O(1D) \rightarrow OH + Cl$	0.99×10^{-10}	Burkholder et al. (2019)
x_{005}	$HCl + O(1D) \rightarrow ClO + H$	3.3×10^{-11}	Burkholder et al. (2019)
x_{006}	$Cl + H_2 \rightarrow HCl + H$	$3.05 \times 10^{-11} e^{-2270/T}$	Burkholder et al. (2019)
x_{007}	$Cl + H_2O_2 \rightarrow HCl + HO_2$	$1.1 \times 10^{-11} e^{-980/T}$	Burkholder et al. (2019)
x_{008}	$Cl + HO_2 \rightarrow HCl + O_2$	$1.4 \times 10^{-11} e^{270/T}$	Burkholder et al. (2019)
x_{009}	$Cl + HO_2 \rightarrow ClO + OH$	$3.6 \times 10^{-11} e^{-375/T}$	Burkholder et al. (2019)
x_{010}	$Cl + O_2 \xrightarrow{M} ClOO$	$k_0 = 2.5 \times 2.2 \times 10^{-33}\left(\frac{T}{300}\right)^{-3.1}$, $k_\infty = 1.8 \times 10^{-10}$	Burkholder et al. (2019)
x_{011}	$Cl + O_3 \rightarrow ClO + O_2$	$2.3 \times 10^{-11} e^{-200/T}$	Burkholder et al. (2019)

Table 1
Continued

ID	Reaction	Rate coefficient	Reference
x_{012}	$Cl + O_3 \xrightarrow{M} ClO_3$	$2.5 \times 1.0 \times 10^{-31}[M]$	Simonaitis and Heicklen (1975)
x_{013}	$Cl + ClOO \rightarrow Cl_2 + O_2$	2.3×10^{-10}	Burkholder et al. (2019)
x_{014}	$Cl + ClOO \rightarrow 2ClO$	1.2×10^{-11}	Burkholder et al. (2019)
x_{015}	$ClO + O \rightarrow Cl + O_2$	$2.8 \times 10^{-11} e^{85/T}$	Burkholder et al. (2019)
x_{016}	$ClO + OH \rightarrow Cl + HO_2$	$7.4 \times 10^{-12} e^{270/T}$	Burkholder et al. (2019)
x_{017}	$ClO + OH \rightarrow HCl + O_2$	$6.0 \times 10^{-13} e^{230/T}$	Burkholder et al. (2019)
x_{018}	$ClO + HO_2 \rightarrow HOCl + O_2$	$2.6 \times 10^{-12} e^{290/T}$	Burkholder et al. (2019)
x_{019}	$ClO + ClO \xrightarrow{M} Cl_2O_2$	$k_0 = 2.5 \times 1.9 \times 10^{-32}(T/298)^{-3.6}$, $k_\infty = 3.7 \times 10^{-12}(T/298)^{-1.6}$	Burkholder et al. (2019)
x_{020}	$ClO + O \xrightarrow{M} OClO$	$k_0 = 2.5 \times 8.6 \times 10^{-21} e^{-420/T} T^{-4.1}$ $k_\infty = 4.33 \times 10^{-11} e^{43/T} T^{-0.03}$	Zhu and Lin (2004)
x_{021}	$ClO + O_3 \rightarrow ClOO + O_2$	$2 \times 10^{-12} e^{-3600/T}$	Burkholder et al. (2019)
x_{022}	$ClO + O_3 \rightarrow OClO + O_2$	$1 \times 10^{-12} e^{-4000/T}$	Burkholder et al. (2019)
x_{023}	$ClO + ClO \rightarrow Cl_2 + O_2$	$1.0 \times 10^{-12} e^{-1590/T}$	Burkholder et al. (2019)
x_{024}	$ClO + ClO \rightarrow ClOO + Cl$	$3.0 \times 10^{-11} e^{-2450/T}$	Burkholder et al. (2019)
x_{025}	$ClO + ClO \rightarrow OClO + Cl$	$3.5 \times 10^{-13} e^{-1370/T}$	Burkholder et al. (2019)
x_{026}	$ClO + ClO_3 \rightarrow ClOO + OClO$	$1.85 \times 10^{-18} e^{-2417/T} T^{2.28}$	Xu and Lin (2003)
x_{027}	$ClO + ClO_3 \rightarrow OClO + OClO$	$1.42 \times 10^{-18} e^{-2870/T} T^{2.11}$	Xu and Lin (2003)
x_{028}	$ClO + ClO_3 \xrightarrow{M} Cl_2O_4$	$k_0 = 2.5 \times 0.143 e^{-1597/T} T^{-10.19}$, $k_\infty = 1.43 \times 10^{-10} e^{-82/T} T^{0.094}$	Xu and Lin (2003)
x_{029}	$ClOO \xrightarrow{M} Cl + O_2$	$2.5 \times 2.8 \times 10^{-10} e^{-1820/T}[M]$	Atkinson et al. (2007)
x_{030}	$ClO_3 + OH \rightarrow HClO_4$	6.67×10^{-13}	Simonaitis and Heicklen (1975)
x_{031}	$ClO_3 + OH \xrightarrow{M} HClO_4$	$k_0 = 2.5 \times 1.94 \times 10^{36} T^{-15.3} e^{-5542/T}$, $k_\infty = 3.2 \times 10^{-10} T^{0.07} e^{-25/T}$	Zhu and Lin (2001)
x_{032}	$ClO_3 + OH \rightarrow OClO + HO_2$	$2.1 \times 10^{-10} e^{-18/T} T^{0.09}$	Zhu and Lin (2001)
x_{033}	$Cl_2 + O(^1D) \rightarrow ClO + Cl$	2.025×10^{-10}	Burkholder et al. (2019)
x_{034}	$Cl_2 + O(^1D) \rightarrow Cl_2 + O$	6.75×10^{-11}	Burkholder et al. (2019)
x_{035}	$Cl_2 + OH \rightarrow HOCl + Cl$	$2.6 \times 10^{-12} e^{-1100/T}$	Burkholder et al. (2019)
x_{036}	$HOCl + O \rightarrow ClO + OH$	1.7×10^{-13}	Burkholder et al. (2019)
x_{037}	$HOCl + OH \rightarrow ClO + H_2O$	$3.0 \times 10^{-12} e^{-500/T}$	Burkholder et al. (2019)
x_{038}	$Cl + HOCl \rightarrow Cl_2 + OH$	$3.196 \times 10^{-12} e^{-130/T}$	Burkholder et al. (2019)
x_{039}	$Cl + HOCl \rightarrow HCl + ClO$	$2.04 \times 10^{-13} e^{-130/T}$	Burkholder et al. (2019)
x_{040}	$Cl + Cl_2O_2 \rightarrow Cl_2 + ClOO$	$7.6 \times 10^{-11} e^{65/T}$	Burkholder et al. (2019)
x_{041}	$Cl_2O_2 \xrightarrow{M} ClO + ClO$	$k_0 = 2.5 \times 3.7 \times 10^{-7} e^{-7690/T}$, $k_\infty = 7.9 \times 10^{15} e^{-8820/T}$	Atkinson et al. (2007)
x_{042}	$OClO + O \rightarrow ClO + O_2$	$2.4 \times 10^{-12} e^{-960/T}$	Burkholder et al. (2019)
x_{043}	$OClO + OH \rightarrow HOCl + O_2$	$1.4 \times 10^{-12} e^{600/T}$	Burkholder et al. (2019)
x_{044}	$Cl + OClO \rightarrow 2ClO$	$3.4 \times 10^{-11} e^{160/T}$	Burkholder et al. (2019)
x_{045}	$OClO + O \xrightarrow{M} ClO_3$	$k_0 = 2.5 \times 3.0 \times 10^{-31}(T/300)^{-3.1}$, $k_\infty = 8.3 \times 10^{-12}$	Burkholder et al. (2019)
x_{046}	$OClO + O_3 \rightarrow ClO_3 + O_2$	$2.1 \times 10^{-12} e^{-4700/T}$	Burkholder et al. (2019)
x_{047}	$Cl_2O_2 + O_3 \rightarrow ClO + ClOO + O_2$	1.0×10^{-19}	Burkholder et al. (2019)

Note. Reaction IDs have been grouped by species: oxygen (a, b), hydrogen (c), carbon monoxide (e), and chlorine (x) respectively. Rate coefficients are $cm^3\ s^{-1}$ for two-body reactions and $cm^6\ s^{-1}$ for three-body reactions. [M] refers to the atmospheric number density (cm^{-3}), and T is temperature (K).

Table 2
Photolysis Reactions Used in This Study, With Sample Photolysis Rates

ID	Reaction	Photolysis rate (s^{-1})	Reference
j_{001}	$O_2 + h\nu \rightarrow O + O$	3.3×10^{-9}	Minschwaner et al. (1992); Yoshino et al. (1988)
j_{002}	$O_2 + h\nu \rightarrow O + O(^1D)$	0.0 (at 40 km)	Brasseur and Solomon (1986)
j_{003}	$CO_2 + h\nu \rightarrow CO + O$	6.8×10^{-11}	Parkinson et al. (2003); B. Lewis and Carver (1983)
j_{004}	$CO_2 + h\nu \rightarrow CO + O(^1D)$	0.0 (at 40 km)	Yoshino, Esmond, Sun, et al. (1996)
j_{005}	$O_3 + h\nu \rightarrow O_2 + O(^1D)$	3.8×10^{-3}	Sander et al. (2006)
j_{006}	$O_3 + h\nu \rightarrow O_2 + O$	6.3×10^{-4}	Sander et al. (2006)
j_{007}	$H_2O + h\nu \rightarrow H + OH$	2.5×10^{-8}	Cheng et al. (1999); Yoshino, Esmond, Parkinson, et al. (1996)
j_{009}	$H_2O_2 + h\nu \rightarrow OH + OH$	4.9×10^{-5}	Schergers and Welge (1968); Sander et al. (2003)
j_{010}	$HO_2 + h\nu \rightarrow OH + O$	3.0×10^{-4}	Sander et al. (2003)
j_{021}	$HCl + h\nu \rightarrow H + Cl$	3.7×10^{-7}	Sander et al. (2006)
j_{022}	$HOCl + h\nu \rightarrow OH + Cl$	2.4×10^{-4}	Barnes et al. (1998)
j_{023}	$ClO + h\nu \rightarrow Cl + O$	2.9×10^{-3}	Trolier et al. (1990)
j_{030}	$Cl_2 + h\nu \rightarrow Cl + Cl$	1.2×10^{-3}	Sander et al. (2006)
j_{031}	$ClOO + h\nu \rightarrow ClO + O$	4.8×10^{-3}	Sander et al. (2011)
j_{032}	$OClO + h\nu \rightarrow ClO + O$	4.0×10^{-2}	Wahner et al. (1987)
j_{033}	$Cl_2O_2 + h\nu \rightarrow Cl + ClOO$	3.4×10^{-3}	Papanastasiou et al. (2009)
j_{034}	$Cl_2O_4 + h\nu \rightarrow ClOO + OClO$	2.2×10^{-4}	Sander et al. (2011)

Note. The sample rates were calculated at an altitude of 40 km above the surface at 0°N, 0°E, at local noon and $L_S \approx 180°$. Equations j_{008}, j_{011}–j_{020} and $j_{024}j_{029}$ involve unsimulated heavy water, nitrogen, organic and sulfur species and so have been excluded.

chlorine species at different altitudes, a variant of the quasi steady-state approximation (Brasseur & Jacob, 2017, p. 264) was applied. In this scheme, the species are sorted by their chemical lifetime and are stepped forward in time using different methods; long-lived species with the SIBEM method, intermediate-lifetime species with an exponential approximation, and short-lived species with a steady-state approximation respectively.

Cl and ClO have short lifetimes as a result of multiple reactions that rapidly inter-convert these two species between each other. As a consequence, the chemical family consisting of the sum of these two species has a long lifetime. We applied the SIBEM method to this "odd-chlorine" family:

$$[ClO_x] = [Cl] + [ClO].$$

Individual species concentrations were then calculated by assuming that ClO is in photochemical equilibrium. A similar approach has been utilized by Lefèvre et al. (2004) when modeling the concentrations of odd-oxygen (O, O_3) and odd-hydrogen (H, OH, HO_2) species on Mars.

2.2. Surface Adsorption Scheme for Perchloric Acid

The chlorine chemistry scheme presented above has perchloric acid ($HClO_4$) as its end product. We investigated the surface distribution of perchlorates of atmospheric origin by implementing a surface deposition scheme to transfer $HClO_4$ from the atmosphere to the surface. We posited the following scheme for the adsorption of gaseous perchloric acid onto the surface regolith:

$$\frac{d[HClO_4]_S}{dt} = \frac{1}{4} \times \gamma \times SSA \times \rho_{soil} \times v_T \times [HClO_4]_A. \quad (1)$$

Here $[HClO_4]_S$ and $[HClO_4]_A$ are the number densities of $HClO_4$ on the surface and in the (≈5 m thick) lowest model layer respectively, γ is the reaction uptake coefficient, $SSA = 1.7 \times 10^4$ m^2 kg^{-1} is the specific surface

area of the Martian soil, $\rho_{soil} = 1650$ kg m^{-3} is the density of Martian soil (both from Gough et al. (2010)). v_T is the thermal velocity of $HClO_4$ at the surface:

$$v_T = \left[\frac{8RT_{air}}{\pi M}\right]^{1/2}, \quad (2)$$

where R is the universal gas constant, T_{air} is the near-surface air temperature and M is the molar mass of $HClO_4$.

No experimentally derived values of the uptake coefficient γ exist for $HClO_4$; therefore, we used a surrogate value of γ that was experimentally measured for CH_4 adsorption onto the surface in Martian conditions by Gough et al. (2010). They estimated that $\gamma = X/(1 + X) \approx X$, where

$$X = \exp(-k_A + k_B/T_{air}), \quad (3)$$

and the fitting parameters are $k_A = 45.41$ and $k_B = 2173.4$. The use of an uptake coefficient that was measured for a different molecule is a significant source of uncertainty in our model, and so in Section 4 we consider the impact of first order variations in the magnitude of the uptake coefficient on estimates of the $HClO_4$ surface adsorption rate.

2.3. Model Configuration

For this study, the MGCM was configured with a spectral truncation at wavenumber 31 (resulting in a 5° latitude-longitude horizontal grid), and with 35 vertical levels extending to around 90 km above the surface. During the simulation, the wind, temperature and surface pressure fields were updated by the dynamical core every 60 s in model time, and the physics and tracer advection routines were called every 10 min. The HCl mass mixing ratio was initialized to 1.2 parts per billion (ppb) by volume (i.e., ≈ 1 ppb by mass) everywhere below approximately 50 km, simulating a well-mixed distribution of HCl in the lower atmosphere where HCl has been detected by the TGO instruments. All other chlorine species were initialized to zero. Data from the OpenMARS reanalysis (Holmes et al., 2020) was used to provide initial conditions for the non-chlorine model fields, and the dust distribution was constrained using the dust maps provided by Montabone et al. (2015, 2020). The model was initialized at $L_S = 159°$ of MY 34, which is the start of the period of TGO observations. The simulation was initially run to the end of MY 34 in order to give the non-HCl chlorine species time to spin-up. We found that equilibrated values were achieved for all species within 100 sols of initialization, with the exception of $HClO_4$ which does not have an atmospheric sink. After the initialization period the model was then run for a further year, over MY 35; the results from this simulation period are reported here.

3. Chlorine Chemistry

Figure 1a shows the mean vertical profiles of the 11 different chlorine species in the model, averaged over MY 35 and over all latitudes and longitudes. HCl is the dominant chlorine species, with a 1-year mean value close to the initialized value of 1.2 ppbv. HCl values decrease slightly above 50 km, in the middle atmosphere, where the monotonically increasing Cl profile reaches its largest abundance. ClO, ClO_3, HOCl and OClO all display parabolic profiles with local maxima occurring at around 40 km. Cl_2O_4 and Cl_2O_2 have monotonically decreasing profiles, and $HClO_4$ has a constant profile at all heights. The ClOO profile increases monotonically from the surface up to 40 km, and then remains relatively constant above that level. The Cl_2 profile is similar, except that it increases toward the surface below 15 km, unlike ClOO.

The averaged profiles of chlorine species discussed above were compared to the previous one-dimensional modeling study of Martian chlorine species by Smith et al. (2014) (their Figure 1c, reproduced in Figure 1b). The overall profile shapes and relative orders of magnitude of HCl and Cl are similar in both works. The profiles of ClO and ClO_3 are similar up to 40 km, but above 40 km both profiles in Smith et al. (2014) decrease rapidly, whereas the comparative decrease is much slower in our results. Also, in our work the amounts of ClO and ClO_3 are comparable, whereas in Smith et al. (2014) they differ by a factor of $\approx 10^3$. The larger amount of ClO_3 results in a larger amount of $HClO_4$ produced in our model than in Smith et al. (2014), although $HClO_4$ is well-mixed in both models. Smith et al. (2014) do not consider seasonal variations in their work, and their one-dimensional model is unable to account for the effects of dynamical and transport processes. Furthermore, they assume an

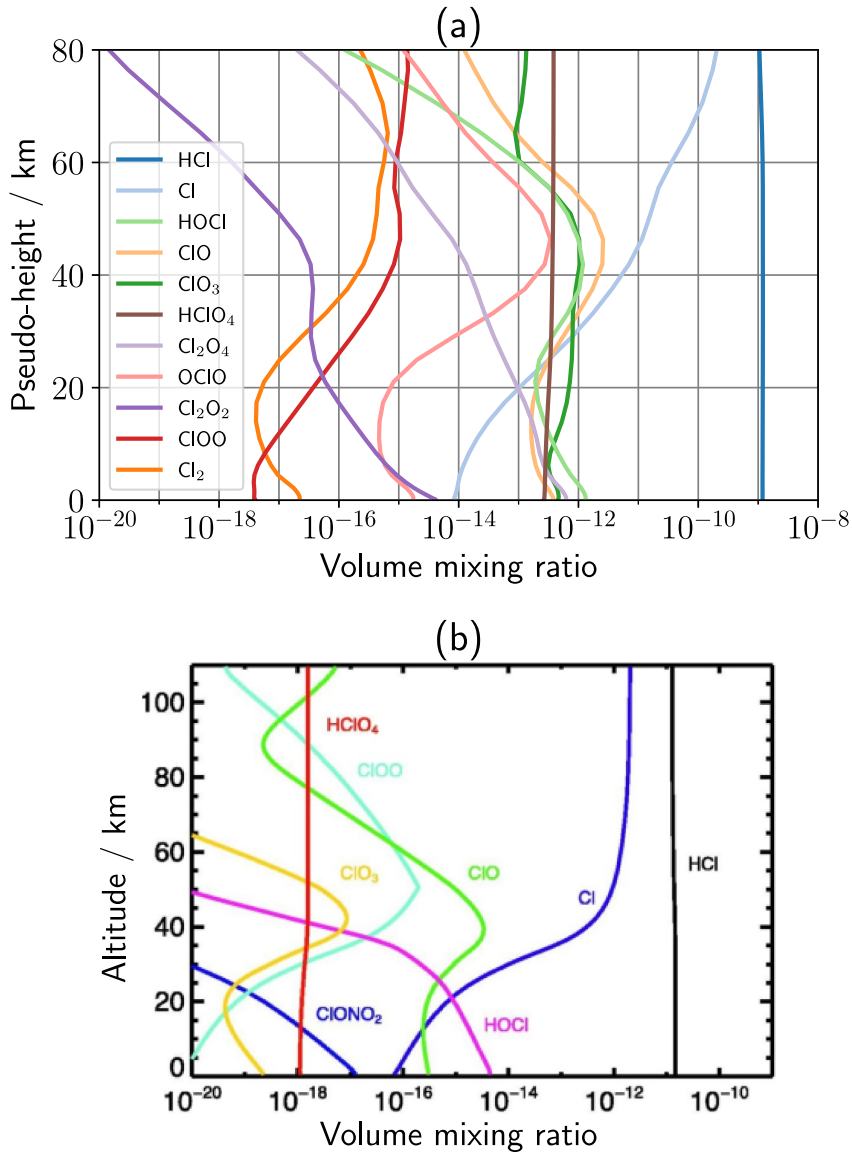

Figure 1. (a) Mean vertical profiles of chlorine species in the Mars Global Climate Model, on a logarithmic scale. The mean profiles were derived by averaging in space (across all longitudes and latitudes) and time (over 1 Martian year of simulation). Model sigma levels were converted to a pseudo-height scale by assuming a fixed scale height of 10.8 km. (b) Vertical profiles of chlorine species from the one-dimensional modeling study of Smith et al. (2014) (their Figure 1c). HCl is introduced via a constant volcanic flux of 6.0×10^4 molec. cm^{-2} s^{-1} and removed via a deposition rate of 0.02 cm s^{-1}. The equilibrium HCl volume mixing ratio is two orders of magnitude smaller than the annual mean value in our study ($\approx 10^{-11}$ vs. $\approx 10^{-9}$) and so, when comparing the figures, all species magnitudes should be rescaled accordingly.

idealized temperature structure (linear decrease to 50 km and constant above that height). There is also less water and ozone in their model above 40 km (Figure S1 in Supporting Information S1); both of these species play key roles in chlorine-related photochemical pathways. These differences between our models are the likely reasons for some of the discrepancies in the species profiles.

Figure 2 presents the spatio-temporal distributions of the main chlorine species that lead to the formation of atmospheric perchloric acid - HCl, Cl, ClO and ClO_3 - at four different times of year. Figure 2 should be considered together with Figure 3, which shows the annual and global mean vertical profiles of the most important production and loss reactions involving the above species. As odd-oxygen and odd-hydrogen species play important roles in the chemistry of these species, the spatial distributions of O, O_3, H_2O, OH and HO_2 are also

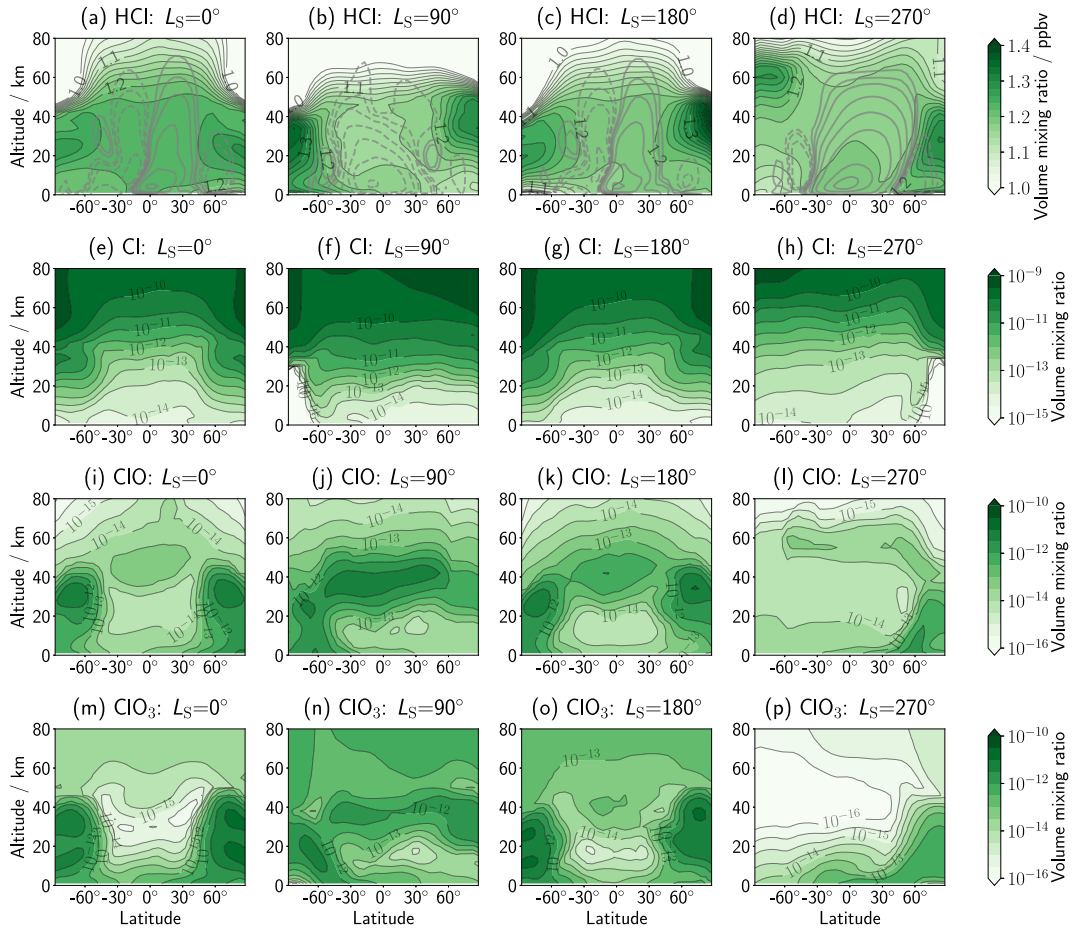

Figure 2. Variations of zonal mean (a–d) HCl, (e–h) Cl, (i–l) ClO, and (m–p) ClO_3 in latitude and altitude (filled contours). Each column displays data that has been time-averaged over a period of 30° of solar longitude centered around L_S = 0°, 90°, 180° and 270° respectively. Note that HCl contour lines have been drawn on a linear scale, compared to a logarithmic scale for the other species. The mean meridional stream function has been included in the HCl subplots as gray contours, with solid (dashed) lines representing anti-clockwise (clockwise) flow along the streamlines.

presented in Figure 4 (see e.g. Lefèvre and Krasnopolsky (2017) for a discussion of these species). The spatio-temporal distributions of the other seven chlorine species, as well as vertical profiles of their major chemical sources and sinks, are presented in the Supplementary Material (Figures S2–S5 and Text S6 in Supporting Information S1).

Figures 2a–2d indicate that HCl values range between 1 and 1.4 ppbv. This relatively small dynamic range indicates that HCl is a well-mixed species and that transport effects generally dominate over chemistry in this work where gas-phase chemistry is being considered exclusively (see P. M. Streeter et al., 2025; Taysum et al., 2024 for the potentially significant role of heterogeneous chemistry). During the equinoxes the Hadley circulation is approximately symmetric, with cells of similar strength in each hemisphere (Figures 2a and 2c). The HCl distribution follows the vertical structure of the cells, with HCl levels reaching higher over the equator due to the tropical upwelling branch of the circulation. Similarly, there is less HCl in the polar regions above 50 km due to the downwelling branches of the Hadley cells (for which direct evidence was recently presented by Olsen, Lefèvre, et al. (2021)) transporting HCl back down to the lower atmosphere. Peak HCl values are found over both poles between 15 and 40 km. Peaks over the poles are also present during the solstices (Figures 2b and 2d), with the peak over the summer pole occurring at a higher altitude than the peak over the winter pole. Low HCl values are present over the summer pole below 20 km. In the tropical regions the HCl distribution is fairly uniform below 40 km, but above that height the HCl volume mixing ratio (vmr) decreases due to an increase in the HCl photolysis rate with height. The vertical extent of the HCl distribution is lowest at northern summer solstice, and is highest

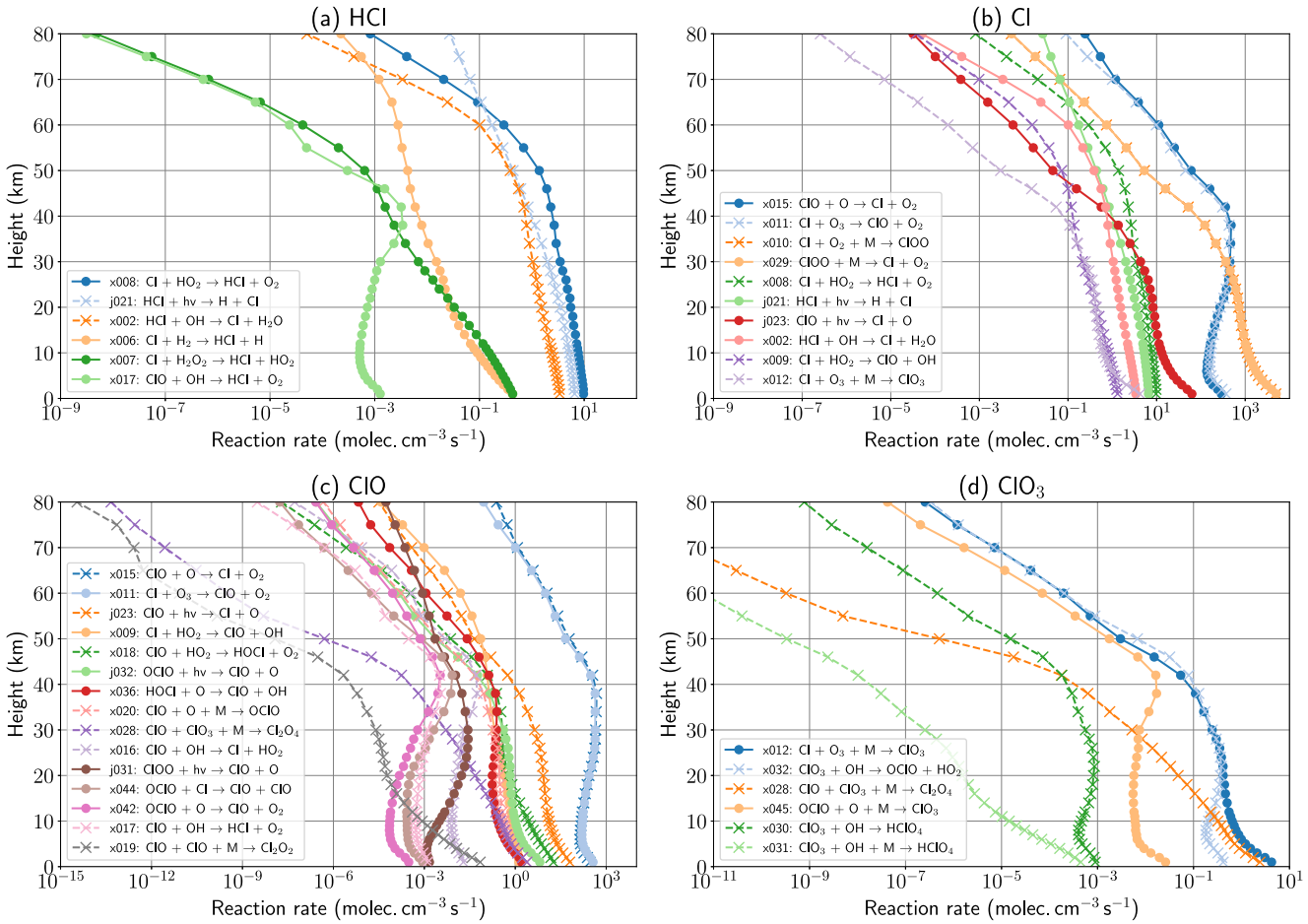

Figure 3. Vertical profiles of selected rates of production and loss for (a) hydrogen chloride, (b) atomic chlorine, (c) chlorine monoxide, and (d) chloride trioxide. Profiles are calculated by averaging each rate equation in space (latitude and longitude) and time (1 Martian year). Filled circles and crosses represent production and loss reactions respectively.

during northern winter solstice; the difference is partly due to differences in the circulations at these times of year, but it is also related to changes in the water cycle, discussed in the next section.

Figure 3a shows the annual and global mean vertical profiles of the most important production and loss reactions involving HCl. The major loss processes of HCl are its conversion to Cl via photolysis (`j021`) and reaction with OH (`x002`). Photolysis is generally the largest loss process, although the loss rates are similar around 40 km where there are significant quantities of OH (cf. Figures 4m–4p). Cl is the most significant source of production of HCl via its reaction with HO_2 (`x008`). Consideration of these reactions explains the peak of HCl over the poles, where photolytic destruction of HCl is reduced, most significantly over the winter pole. At the same time, HCl is produced at around 40 km by the reaction of significant amounts of HO_2 (Figures 4q–4t)—formed by the reaction of downwelling H atoms with O_2—with downwelling Cl atoms. During the solstices, the HCl peak over the summer pole is advected upwards, and so the altitude of the HCl peak is higher over the summer pole than the winter pole (Figures 3b and 3d). The increase in the amount of HO_2 in the atmosphere during the warm perihelion season also explains the differences in the amounts of HCl above 60 km during northern winter solstice compared to northern summer solstice, as the increased quantity of HO_2 during northern winter solstice reacts with Cl to form more HCl in the middle atmosphere.

Figures 2e–2h shows the latitude-height distribution of atomic chlorine (Cl). The Cl distribution is much more variable than HCl, and its vmr increases exponentially with height from 10^{-14} near the surface to 10^{-10} at around 60 km. During the equinoxes (Figures 2e and 2g), the Cl distribution is symmetric about the equator with the largest values occurring over both poles above 50 km. During the solstices (Figures 2f and 2h), the Cl vmr over the

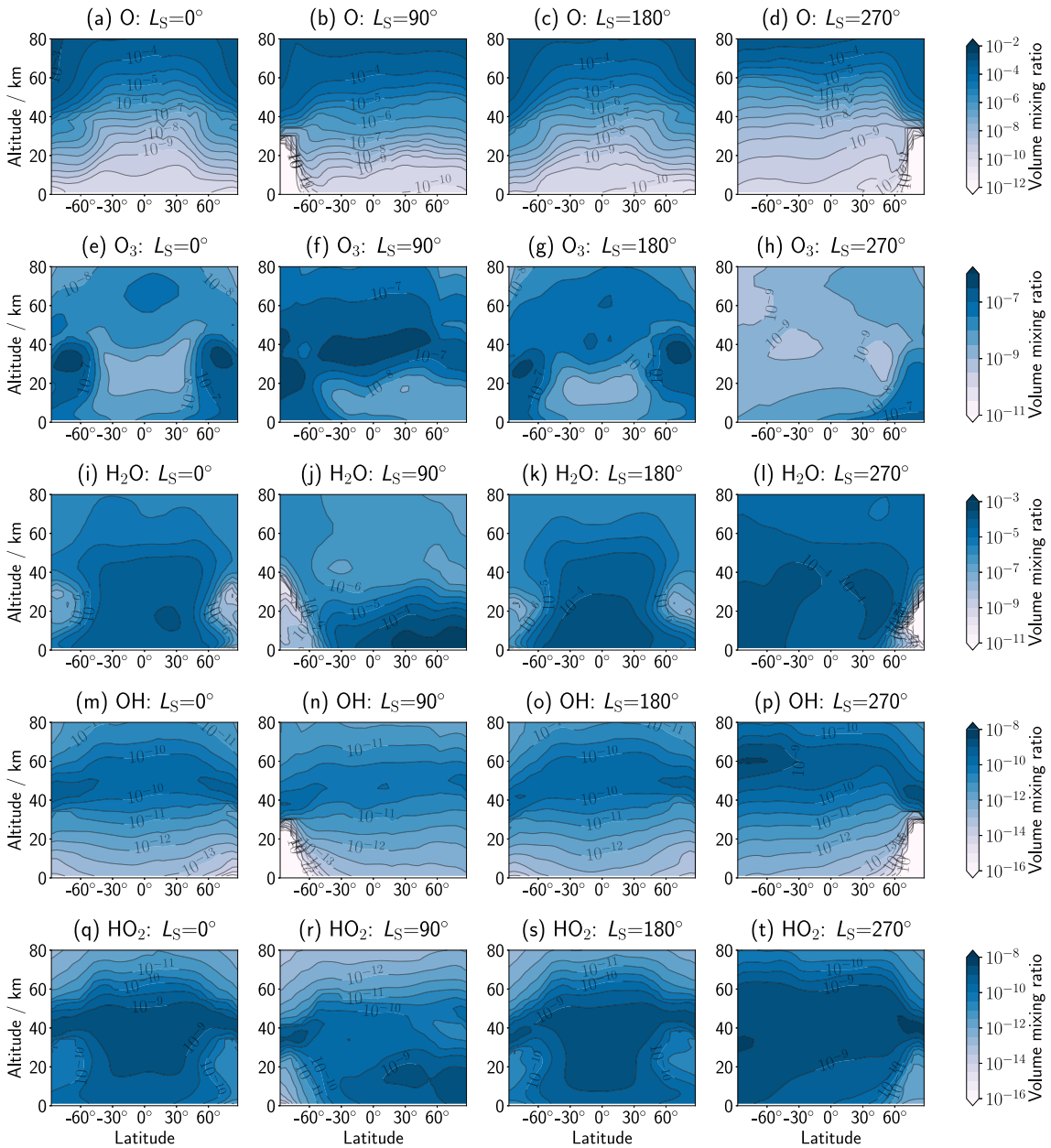

Figure 4. Variations of zonal mean (a–d) atomic oxygen, (e–h) ozone, (i–l) water, (m–p) hydroxyl, and (q–t) hydroperoxyl in latitude and altitude. Each column displays data that has been time-averaged over a period of 30° of solar longitude centered around L_S = 0°, 90°, 180° and 270° respectively.

winter pole drops to very low values below 40 km; at the same time, maximum values of Cl are to be found over each winter pole above 40 km, driven by downwelling of the single-cell Hadley circulation.

The major production and loss rates for Cl and ClO are given in Figures 3b and 3c. As described in Section 2.1, these two species undergo rapid inter-conversions and are therefore modeled as a single family, ClO_x, which has a longer lifetime than each constituent species. The major production mechanisms of the ClO_x family are the production of Cl from HCl via photolysis (`j021`) and reaction of HCl with OH (`x002`), as previously discussed. Production of Cl via the breakdown of chlorine peroxy (ClOO) is also large (`x029`), but is almost completely balanced by the reverse reaction (`x010`) and so is discounted. The main loss process for the ClO_x family is the reaction of Cl with HO_2 to produce HCl (`x008`).

The proportions of Cl and ClO within the ClO_x family are determined by assuming that ClO is in photochemical equilibrium, that is, that its production and loss rates are balanced. Consideration of only the dominant production and loss mechanisms yields the following approximate expression:

$$[ClO] = \frac{\text{ClO Production}}{\text{ClO Loss}} \approx \frac{k_{x011}[Cl][O_3]}{k_{x015}[O]}. \quad (4)$$

Here k_{x011} denotes the rate coefficient for the reaction of Cl and O_3 to produce ClO and O_2 (x011), and k_{x015} is the rate coefficient for the reaction of ClO with O to produce Cl and O_2 (x015). This expression highlights the key role played by odd-oxygen species in controlling the balance of Cl and ClO in the atmosphere. The presence of O_3 enhances the balance of the family toward ClO via (x011); conversely, the presence of O atoms reduces the amount of ClO via (x015).

The greater amount of Cl above 40 km during northern summer solstice compared to northern winter solstice can be attributed to the significantly reduced amounts of HO_2 in the atmosphere during the cold aphelion period, allowing for a greater buildup of Cl. The significant decrease in Cl levels in the winter polar region during the solstices (Figure 2 (f,h)) is due to the lack of sunlight and very low values of OH in the winter polar regions (Figures 4n and 4p), which together curtail the replenishment of Cl via destruction of HCl. At the same time, the build-up of O_3 in the same region (Figures 4f and 4h), together with the absence of O in the winter extratropics (Figures 4b and 4d), encourages the conversion of Cl to ClO via equation (x011) whilst preventing the reverse reaction (x015).

Figures 2i–2l shows the latitude-height distribution of chlorine monoxide (ClO). Equation 4 implies that the $[ClO]/[Cl]$ ratio is directly proportional to the $[O_3]/[O]$ ratio, to a first approximation, since variations in k_{x011}/k_{x015} are comparatively small. Since the spatial distributions of Cl and O are very similar (compare Figures 2e–2h and 4a–4d), the distribution of ClO (Figures 2i–2l) is strongly correlated with the O_3 distribution (Figures 4e–4h). At the equinoxes, peak values of ClO occur over the poles between 0 and 40 km and at the equator at 40 km; these are regions where there is a build-up of O_3 (Figures 2i and 2k). Above these heights the amount of ClO decreases due to the rapid increase in O and thus destruction of ClO via (x015). The ClO distribution during the solstices (Figures 2j and 2l) also follows the corresponding O_3 distributions (Figures 2f and 2h) closely, with a buildup over the winter pole and a peak in the tropics at 40 km during northern summer solstice.

The latitude-height distribution of ClO_3 is given in Figures 2m–2p, and the major production and loss mechanisms for ClO_3 are shown in Figure 3d. The most important production process for ClO_3 is the reaction of Cl with O_3 (x012), and the largest loss process is the reaction of ClO_3 with OH (x032). As a result, the spatial distribution of ClO_3 is closely related to the distributions of O_3 and OH. During the equinoxes ClO_3 is high over both poles where there is a maximum in O_3 and relatively little OH (Figures 2m and 2o), and for similar reasons during the solstices ClO_3 peaks over the winter pole (Figures 2n and 2p). There is also much less ClO_3 in the atmosphere during northern winter than northern summer due to there being comparatively more OH and less O_3 in the atmosphere during northern winter.

4. Surface Distribution of Perchlorate

$HClO_4$ is formed from ClO_3 and OH via (x030) and (x031); as its formation rate is slow, it is a relatively well-mixed gas in the atmosphere (see Figures S3m–S3p in Supporting Information S1). Figure 5a shows variations in the surface $HClO_4$ adsorption rate across latitude and time, over the course of MY 35. There is a clear seasonal structure, with the bulk of the adsorption occurring in the extratropical regions during the respective winter seasons. Comparatively little surface adsorption occurs outside of these latitudes and times. The total mass of chlorine adsorbed on the surface over the year was found to be approximately 2,600 kg. Given that the total mass of chlorine initialized in the model is 2.6×10^7 kg, and assuming a constant annual adsorption rate, we estimate that it would take approximately 10,000 years to remove all of the chlorine from the atmosphere via this mechanism.

Figure 5b shows the spatial distribution of surface $HClO_4$ after 1 Martian year (MY 35). The surface distribution of $HClO_4$ shows a strong latitudinal dependence, with the largest deposits occurring in polar regions, particularly

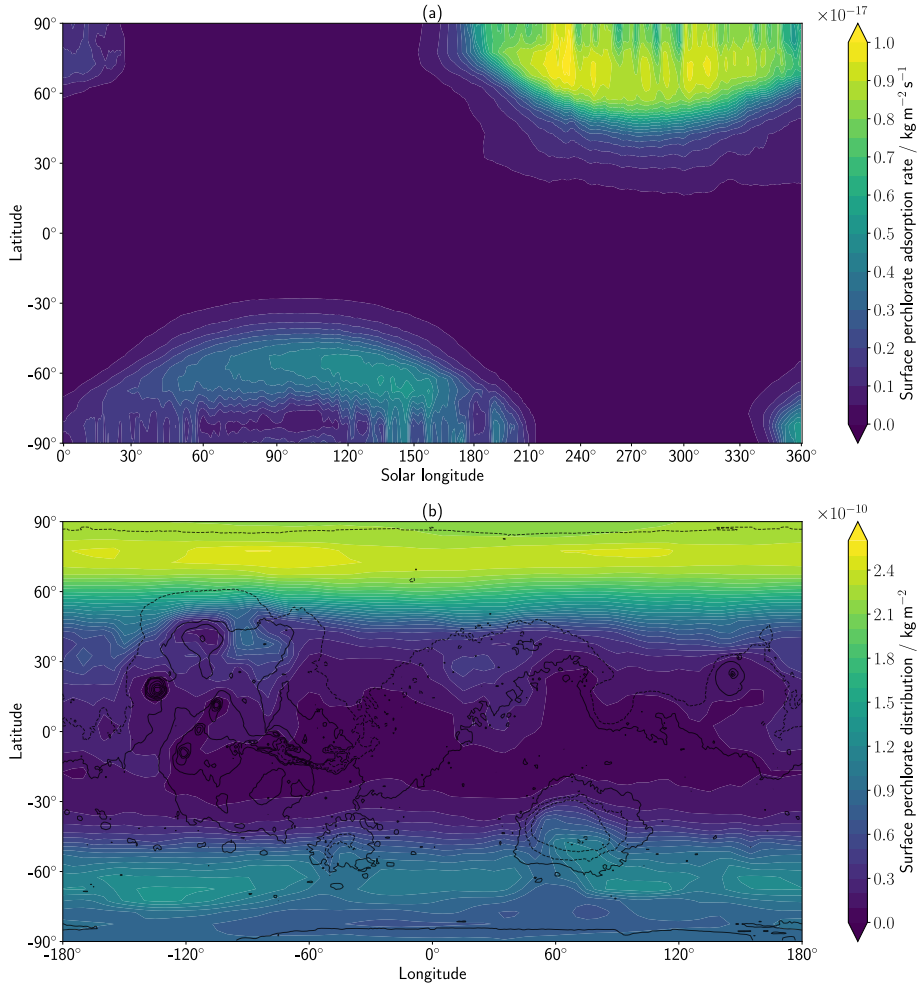

Figure 5. (a) Variation of the surface perchlorate adsorption rate across latitude and solar longitude. The data has been smoothed by applying a 3-sol running mean. (b) Spatial distribution of cumulative surface $HClO_4$ deposits over the course of Mars Year 35.

the northern polar region. In the northern extratropics, the largest deposits occur in a band centered around 75°N. There is a slight longitudinal asymmetry, with greater adsorption having occurred in the region northeast of Alba Patera (regions are labeled in Figure 6). There is less adsorption over the course of the year in the southern extratropics compared to the north; this is partly because the amount of perchlorate is increasing in the model, and so a larger amount is available for adsorption during northern winter than during southern winter for the chosen study period $L_S = 0°–360°$ of MY 35. However, topographic differences between the hemispheres also play a role; these will be discussed later in this section.

Figure 6a shows the distribution of surface $HClO_4$ in the tropics. The model distribution of perchlorates can be compared to the distribution of chlorine measured by the GRS aboard the Mars Odyssey spacecraft (Keller et al., 2006), shown in Figure 6b. The plots show a broad similarity in longitudinal structure, with enhancements of chlorine in the Medusae Fossae, Tharsis and Arabia Terra regions, and reduced amounts of chlorine in the southern tropics. However, there are also differences: for example, the GRS data shows reduced amounts Cl in the Hellas and Utopia Planitia regions, but these are regions with significant perchlorate deposits in the model.

The spatial distribution of surface perchlorate is influenced by near-surface air temperature and $HClO_4$ number density (cf. Equation 1); annual-mean quantities of these two fields are shown in Figures 7a and 7b. The variations in the tropical perchlorate distribution seen in Figure 6a are broadly reflected in the variations in the mean near-surface temperature (Figure 7a); given the negative temperature dependence of the uptake coefficient

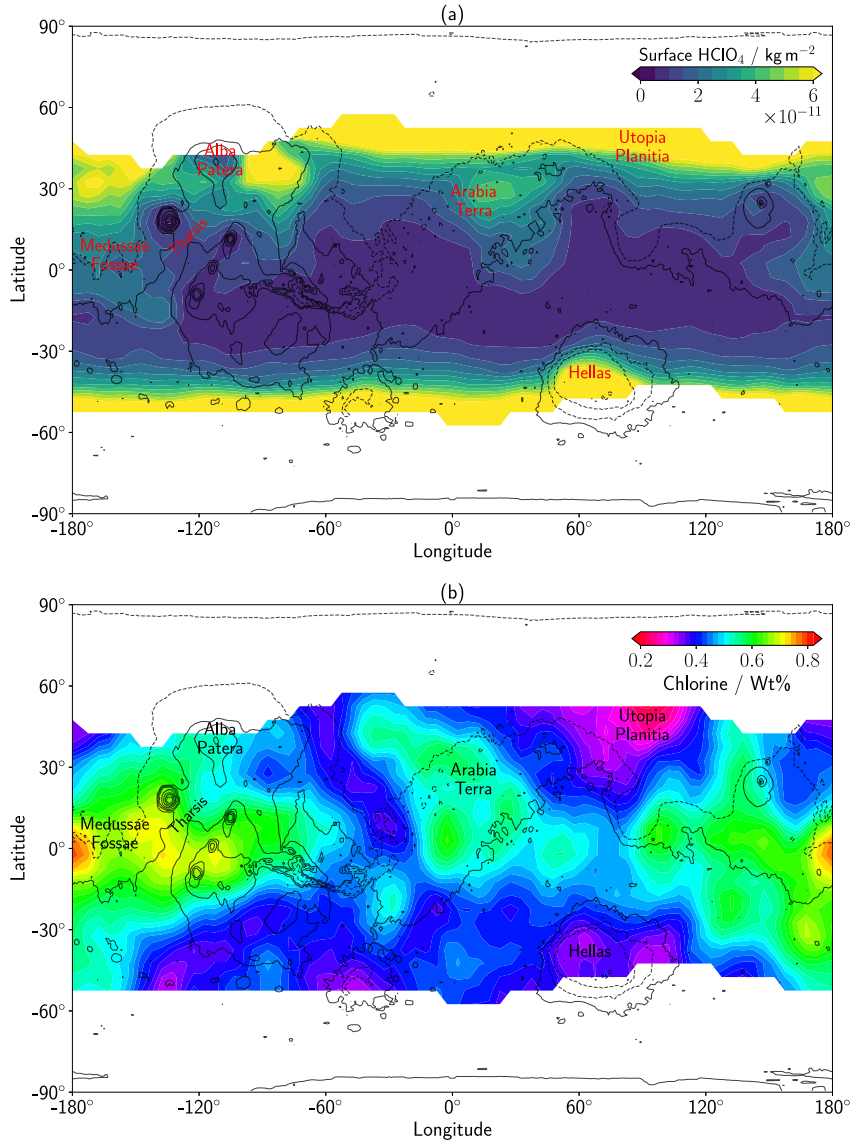

Figure 6. (a) Spatial distribution of cumulative surface $HClO_4$ deposits in the tropics. This plot uses the same data as Figure 5 (b), but the color scale has been enhanced and the data has been masked for comparison with observations. (b) Surface distribution of Cl (in weight %) as measured by the Gamma Ray Spectrometer on board Mars Odyssey, based on data from Keller et al. (2006).

(Equation 3), areas with lower temperatures have larger deposits of $HClO_4$. The difference between adsorption rates in the northern and southern extratropics can be explained by differences in the near-surface $HClO_4$ number density (Figure 7b); this is much higher in the northern high latitudes than in the southern high latitudes due to the topographic asymmetry between the hemispheres, and so greater adsorption occurs in the north.

Variations in the near-surface temperature are closely linked to the thermal inertia of the underlying Martian surface, which is shown in Figure 7c. Areas with low thermal inertia correspond to areas where surface adsorption is high, and longitudinal variations in the thermal inertia field correlate with longitudinal variations in the surface perchlorate distribution. The sensitivity of the perchlorate field to thermal inertia variations reflects the nonlinear (exponential) dependence of the uptake coefficient γ to changes in temperature; for example, regions with low

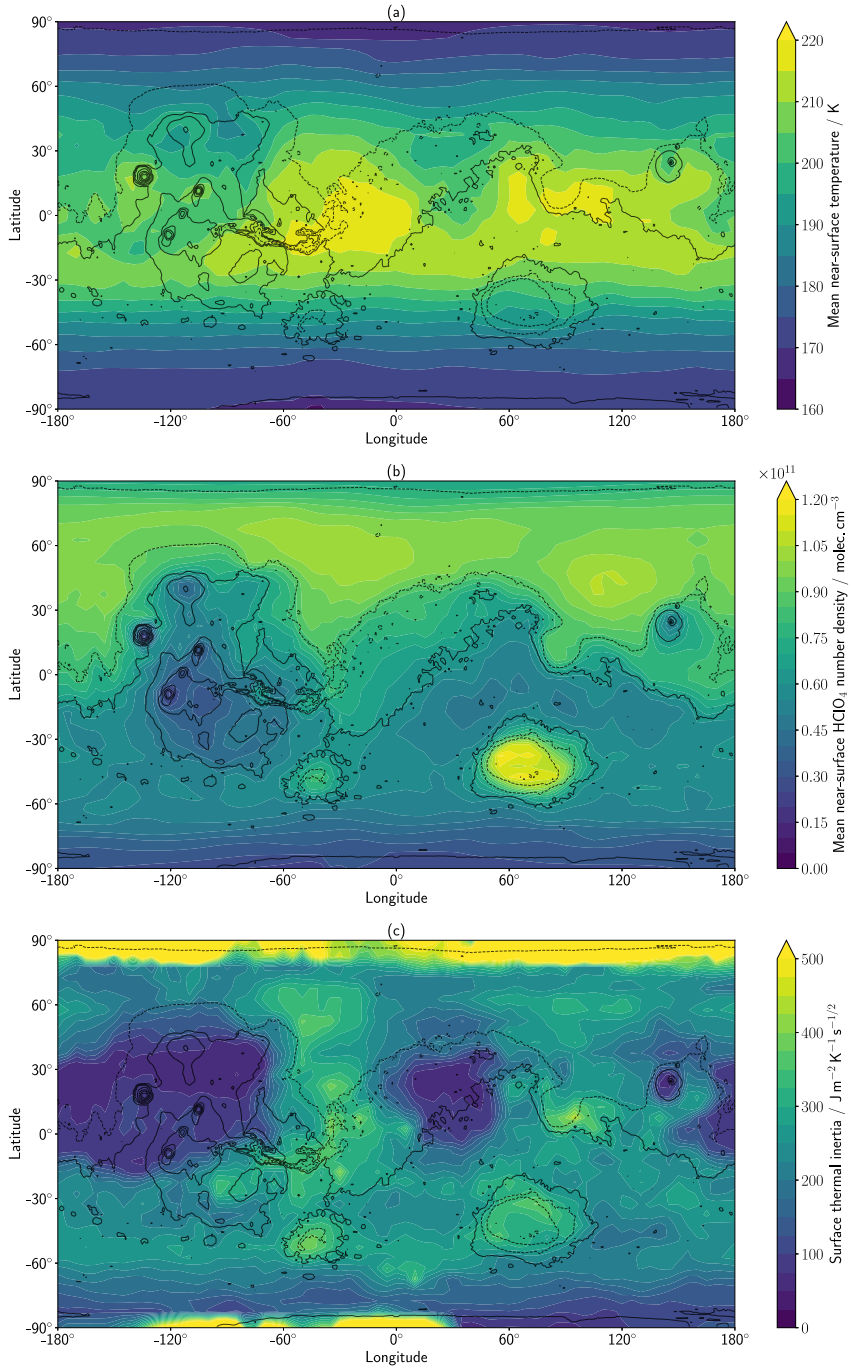

Figure 7. Spatial distributions of (a) near-surface air temperature, (b) near-surface $HClO_4$ number density, and (c) surface thermal inertia. The near-surface air temperature and $HClO_4$ number density fields have been averaged over a Martian year.

thermal inertia will exhibit a larger diurnal cycle, and therefore $HClO_4$ adsorption will be much larger in these regions at night compared to neighboring regions with the same mean temperature but greater thermal inertia.

We briefly examined the impact of applying the adsorption scheme to other chlorine species. Figure S7 in Supporting Information S1 shows the outcome of a model simulation where the surface adsorption scheme was applied to HCl rather than $HClO_4$, using the same adsorption parameters. The resulting spatial distribution of surface deposits of hydrogen chloride mirrors that of the perchlorate distribution (albeit with much larger magnitudes; compare Figure 5), since both gases are relatively well-mixed in the atmosphere. However, the

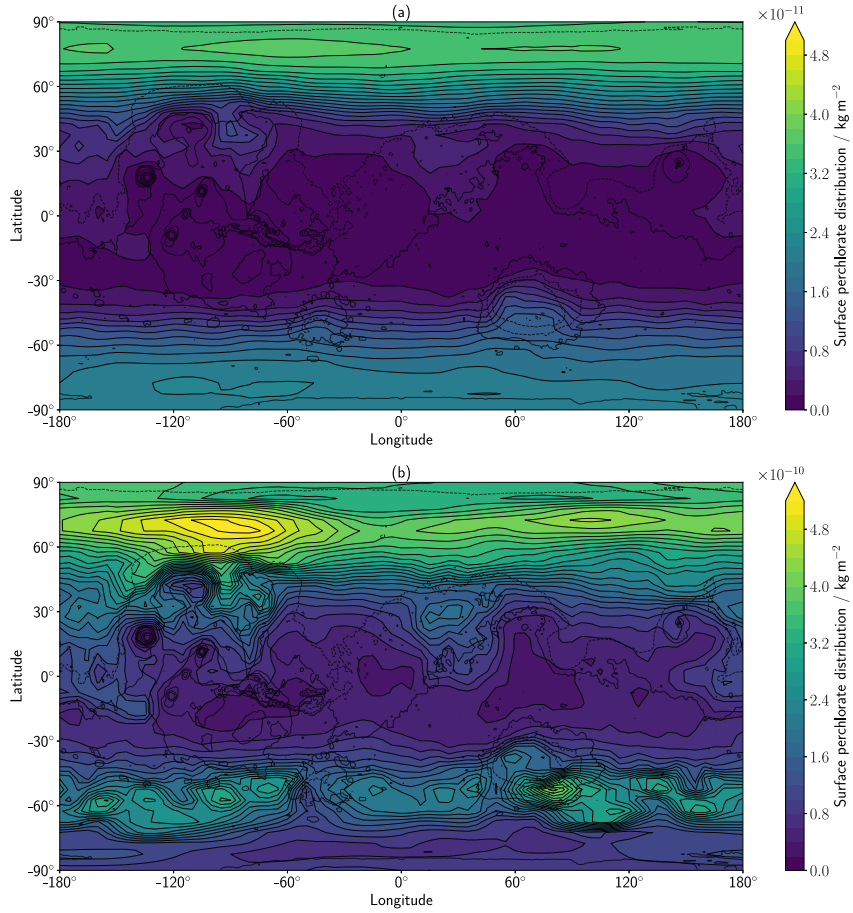

Figure 8. Spatial distribution of surface perchlorate accumulation over the course of MY 35, under variations of the uptake coefficient $\gamma \approx \exp(-k_A + k_B/T)$: (a) $k_A = 47.71$, (b) $k_A = 43.11$, representing an order of magnitude increase and decrease in γ respectively compared to Figure 5a. The value of k_B is kept constant at $k_B = 2173.4$.

hemispheric asymmetry in extratropical deposits of HCl is less pronounced compared to $HClO_4$ (compare Figure 5b and Figure S7b in Supporting Information S1)—this is because the amount of HCl in the model remains relatively constant over the course of 1 Martian year, whereas the amount of $HClO_4$ increases significantly over the same period.

We investigated the sensitivity of the surface perchlorate distribution to changes in the temperature-dependent uptake coefficient γ (cf. Equation 3). Two additional model simulations were performed that were identical to the original simulation but with the value of k_A set to $k_A = 47.71$ and $k_A = 43.11$; these values were selected in order to respectively decrease and increase the value of γ by a factor of 10 with respect to the high-temperature limit of γ used in the original simulation. The value of k_B was fixed at $k_B = 2173.4$.

When γ was reduced by an order of magnitude (Figure 8a), the mass of perchlorate deposits decreased by an order of magnitude, and the total amount of chlorine adsorbed onto the surface reduced to 370 kg. However, most of the features noted in Figure 5b remain: there is a clear preference for adsorption to occur in the extratropics, and within the tropics slightly more adsorption occurs in the Medusae Fossae, Alba Patera and Arabia Terra regions mentioned previously. However, the relative magnitudes of these features are reduced. When γ was increased by an order of magnitude (Figure 8b), the same spatial pattern of perchlorate adsorption is preserved and enhanced: along with adsorption at the regions previously mentioned, there is an evident increase in adsorption in the area north of Alba Patera, as well as in the southern extratropics (such as in the south-east corner of the Hellas basin). The total amount of chlorine adsorbed onto the surface in this case is 7,300 kg.

5. Discussion

The surface distribution of perchlorate over a year of simulation indicates that perchloric acid adsorption occurs preferentially in the polar regions (Figures 5b and 8, Figure S7b in Supporting Information S1) for our chemistry scheme that considers only gas-phase reactions of atmospheric chlorine species. The surface adsorption scheme introduced here has a negative temperature dependence, with adsorption occurring preferentially on cold areas of the surface. Lower elevation levels in the northern extratropics further enhance surface adsorption, due to increased near-surface $HClO_4$ number densities. We have shown that a similar surface distribution arises when the parameter γ is increased or decreased by an order of magnitude (Figure 8), and when the adsorption scheme is applied to HCl (Figure S7 in Supporting Information S1). This suggests that the surface distributions presented in this work could potentially apply to any well-mixed atmospheric species with a temperature-dependent uptake coefficient.

It is notable that the surface distribution predicts relatively high levels of perchlorate deposits at the location of the Phoenix lander (68°N, 126°W), where high levels of perchlorate salts were measured (Hecht et al., 2009). Our modeling results thus suggest that if surface perchlorates form primarily through the atmospheric pathway explored here, then the perchlorate levels measured by the Phoenix lander may be quite high relative to other places on the surface, and so may not be representative of the planet as a whole.

The total mass of chlorine that deposited (as perchlorate) onto the surface over the course of one Mars year was found to vary between 370 and 7,300 kg, depending on the particular choice of the uptake coefficient γ. Assuming that the same rate of adsorption is maintained each year, we estimate that it would take between 10^3–10^5 years to remove 1 ppbv of HCl from the Martian atmosphere via the surface adsorption of atmospheric perchloric acid, with the bulk of the adsorption occurring in the polar regions. This estimate could be narrowed by experimental work characterizing the specific adsorption parameters of chlorine species onto rocky and icy surfaces. However, it is also subject to the uncertainties of the chemical production rates of ClO_3 and $HClO_4$ (equations `x012` and `x030` respectively), as well as model uncertainty - for example, we have not considered the impact of desorption of gases back into the atmosphere. Furthermore, heterogeneous interactions between gas-phase species and atmospheric aerosols could further enhance perchlorate production; for example, it has been shown by McKeachie et al. (2004) that ClO can react on ice when the ice sublimates, producing OClO that serves as an additional source of perchlorate via equations `x045`–`x046` and `x030`–`x031`. Therefore, the above estimates must be considered to be preliminary and subject to further refinement.

In the tropics, our work predicts enhanced surface adsorption in the Medusae Fossae, Tharsis and Arabia Terra regions. Our findings are broadly consistent with the measurements of near-surface chlorine by the GRS on board the Mars Odyssey spacecraft (Keller et al., 2006), which show elevated chlorine values in those same locations. In our model, enhanced adsorption is closely linked to near-surface temperature and surface thermal inertia (Figures 7a and 7c). Keller et al. (2006) noted a negative correlation between the observed surface chlorine distribution and surface thermal inertia; our work points toward a possible causal link between this observation, via preferential adsorption of atmospheric chlorine species at regions with low thermal inertia. Keller et al. (2006) also noted that the observed Cl distribution had a significant positive correlation with the distribution of H, and a negative correlation with the distribution of Si. We speculate that these correlations may be related to the differences in uptake of atmospheric chlorine species onto icy and rocky surfaces. Future experimental work will be crucial to improving the characterization of the adsorption process for different chlorine species on different surfaces.

However, the GRS results also show low amounts of chlorine in the southern subtropical latitudes around 50°, as well as in part of Utopia Planitia (Figure 6b); neither of these features are present in our model results. The surface adsorption model that we have used also contains several parameters that are not well-constrained, most significantly the exact uptake coefficient of $HClO_4$ which has not been measured experimentally. We have also not considered the impacts of obliquity variations on surface adsorption; given the potentially long timescale of 10^5 years over which surface adsorption happens, this could be an important factor.

It is possible that the observed negative correlation between surface chlorine and thermal inertia is primarily driven by other processes rather than surface adsorption of atmospheric chlorine. For example, it is believed that low thermal inertia surfaces on Mars correspond to dusty surfaces (e.g., Kieffer et al., 1977). Therefore, if there was a mechanism by which chlorine could be incorporated into the dust—such as via a heterogeneous interaction

between dust and HCl, as reported to occur on Earth by Sullivan et al. (2007)—then this could be responsible for the correlation between (high dust) thermal inertia areas and chlorine-rich areas. Evaluation of this possibility could be the subject of a future study.

In our model simulation we used an initially uniform HCl distribution of 1.2 ppbv everywhere below approximately 50 km. Whilst this is not a realistic initial condition, we find it acceptable within the context of gas-phase chlorine chemistry modeling because of the long atmospheric lifetime of HCl under these conditions; most particularities of the initial HCl distribution quickly become smoothened out as the gas is transported and mixed within the atmosphere, resulting in an approximately uniform distribution. However, latitudinal mixing is expected to be limited in the polar winter region where the fast-moving jet stream restricts the movement of air masses into and out of the polar vortex. The effects of this transport barrier, while still present, may not be as clear in our simulations due to the assumed uniformity of the initial HCl distribution.

Of course, in the real atmosphere the initial HCl distribution will depend on the locations of the sources and sinks of HCl, and identifying these remains the subject of ongoing research. Once the physical processes controlling the production and loss of HCl have been confirmed, it would be worthwhile to explore more realistic initial and boundary conditions to the model. One possibility could be to introduce HCl via point surface emissions in areas of geologically recent tectonic activity such as Tharsis (Hauber et al., 2011) and Elysium Planitia (Broquet & Andrews-Hanna, 2023), to investigate the effects of atmospheric transport on HCl emissions from volcanic sources and the resulting surface distribution of perchlorates.

HCl in our model does exhibit seasonal variations, the most significant of which occurs in the polar regions. There, HCl is relatively enhanced over the winter pole, driven by the interaction between HO_2 and downwelling Cl atoms. This interaction has not been described in previous one-dimensional modeling studies of Martian HCl, as these works would have been unable to resolve the downward transport of Cl atoms without use of a full MGCM. However, the seasonal evolution of HCl in our model does not agree well with the recent observations of HCl by instruments aboard the ExoMars TGO (Aoki et al., 2021; Korablev et al., 2021; Olsen, Trokhimovskiy, et al., 2021). A clear feature of the observations has been a distinct seasonal pattern in the prevalence of HCl. Almost all detections of HCl have occurred during the perihelion season, and there have been very few positive detections of HCl during the cold aphelion season in either hemisphere despite clear observation conditions (see Figure 5 of Olsen, Trokhimovskiy, et al. (2021)). The effective disappearance of HCl during the aphelion season is absent in our model; whilst there is indeed a seasonal cycle of HCl in our simulation, seasonal variations do not exceed ≈ 20% of the annual-mean HCl value (Figures 2a–2d). Chlorine removal via surface adsorption of $HClO_4$ also does not have an appreciable effect on HCl levels over a year compared to the scale of the changes observed by the satellite instruments. It is likely that heterogeneous processes, recently studied in one-dimensional models by Krasnopolsky (2022) and Taysum et al. (2024) but not simulated in this work, are responsible for the observed seasonal changes in the HCl distribution.

Despite the above limitations, our model simulation still provides useful insights into the distribution of the other non-HCl species. The detection limit of HCl observations is around 0.1 ppbv, and so it is possible that there are small amounts of HCl well-mixed throughout the atmosphere; this should be sufficient to reproduce the qualitative distributions of the other non-HCl species, if not the exact quantities. We have shown that the distributions of the major chlorine species are strongly impacted by odd-oxygen and odd-hydrogen species. OH and HO_2 molecules play a significant role in mediating the concentration of Cl. Similarly, the balance between Cl and ClO is primarily controlled by the presence of O_3 and O, with HO_2 exerting a secondary influence. There is a very strong correlation between O_3 and ClO distributions throughout the year, and especially during aphelion (compare Figures 2j and 4f). Since all of the other chlorine species explored in this scheme are sourced from either Cl or ClO, the influence of the odd-hydrogen and odd-oxygen species on the distribution and evolution of chlorine species is pervasive.

One implication of this work is that observations of HCl can in principle be used, together with O_3 and H_2O, to help constrain the odd-hydrogen chemistry that is so crucial for maintaining the stability of the Martian atmosphere, but whose exact nature still eludes understanding. However, this would require an improved representation of the seasonal variability of HCl, which we have shown that gas-phase chemistry alone cannot reproduce. In a companion work (P. M. Streeter et al., 2025) we investigate the impact of heterogeneous chemistry on the surfaces of dust and ice aerosols on chlorine species; this has been suggested as a possible explanation for the observed seasonal variations in the HCl distribution (Korablev et al., 2021; Krasnopolsky, 2022; Olsen,

Trokhimovskiy, et al., 2021; Taysum et al., 2024). The results in this paper constitute a useful benchmark against which that work and other future investigations can be compared. It is also noteworthy that many of the chlorine species studied here tend to have the highest concentrations in the high extratropics, especially in the winter hemispheres. Given the presence of water ice clouds in these regions, and the recent findings of Olsen et al. (2024b) of an anti-correlation between HCl and water ice profiles in TGO observations between 40 and 50 km, it seems increasingly likely that heterogeneous chemistry plays an important role in the Martian chlorine cycle, just as it does on Earth (Solomon, 1999).

6. Conclusion

We have used a global climate model to investigate the spatial and seasonal distributions of chlorine species in the Martian atmosphere, as well as the distribution of perchlorate resulting from the adsorption of atmospheric perchloric acid onto the surface. We found that the chemistry of odd-oxygen and odd-hydrogen species plays a large mediating role in the distribution of chlorine species; in particular, there is a strong correlation between the distributions of Cl and ClO with O and O_3 respectively. We also found that the HCl distribution is predominantly controlled by dynamical effects, especially at the poles during equinox and the winter pole during solstice where reactions between downwelling Cl and HO_2 species creates a local maximum in the HCl distribution. We found encouraging agreement between the surface distribution of perchlorate in our model with both in situ and remote observations, and we found that surface thermal inertia, together with near-surface temperature and topography, plays a significant role in controlling the locations of these deposits. However, our model was unable to reproduce the distinct seasonal cycle of HCl that has been observed by instruments aboard the TGO, reflecting the need for the inclusion of heterogeneous processes. Our MGCM study suggests that the atmospheric origin theory of Martian surface perchlorates posited by Catling et al. (2010) could indeed be a viable mechanism for explaining the observed distribution of surface chlorine, and it highlights the pressing need for better experimental constraints on the processes controlling surface-atmosphere exchange of chlorine species.

Data Availability Statement

Data - Data fom the GRS is hosted on the NASA Planetary Data System archive (Boynton, 2007). Outputs from the MGCM used in this study have been uploaded to the Open Research Data Online repository (Rajendran et al., 2024).

Acknowledgments
KR, PMS, SRL and MRP acknowledge funding from the UK Space Agency (UKSA) under grant ST/W002949/1. MRP also acknowledges funding from UKSA through grants ST/V002295/1, ST/Y006054/1, ST/Y005929/1, ST/X006549/1 and ST/Y000234/1. JAH acknowledges funding from the UKSA under grants ST/W00268X/1 and ST/R001405/1, and from STFC under grant ST/X001180/1. KSO acknowledges funding from the UKSA under grants ST/T002069/1 and ST/Y000196/1. OK acknowledges funding from Roscosmos and the Ministry of Science and Education in Russia.

References

Aoki, S., Daerden, F., Viscardy, S., Thomas, I., Erwin, J., Robert, S., et al. (2021). Annual appearance of hydrogen chloride on Mars and a striking similarity with the water vapor vertical distribution observed by TGO/NOMAD. *Geophysical Research Letters*, *48*(11), e2021GL092506. https://doi.org/10.1029/2021GL092506

Aoki, S., Faggi, S., Villanueva, G., Liuzzi, G., Sagawa, H., Daerden, F., et al. (2024). Global mapping of HCl on Mars by IRTF/iSHELL. *The Planetary Science Journal*, *5*(7), 158. https://doi.org/10.3847/PSJ/ad58dc

Atkinson, R., Baulch, D., Cox, R., Crowley, J., Hampson, R., Hynes, R., et al. (2007). Evaluated kinetic and photochemical data for atmospheric chemistry: Volume III–gas phase reactions of inorganic halogens. *Atmospheric Chemistry and Physics*, *7*(4), 981–1191. https://doi.org/10.5194/acp-7-981-2007

Barnes, R., Sinha, A., & Michelsen, H. (1998). Assessing the contribution of the lowest triplet state to the near-UV absorption spectrum of HOCl. *Journal of Physical Chemistry A*, *102*(45), 8855–8859. https://doi.org/10.1021/jp9835869

Baulch, D., Bowman, C., Cobos, C., Cox, R., Just, T., Kerr, J., et al. (2005). Evaluated kinetic data for combustion modeling: Supplement II. *Journal of Physical and Chemical Reference Data*, *34*(3), 757–1397. https://doi.org/10.1063/1.1748524

Boynton, W. (2007). Mars Odyssey gamma ray spectrometer element concentration data V1.0 [Dataset]. *NASA Planetary Data System*. https://doi.org/10.17189/1519480

Brasseur, G., & Jacob, D. (2017). *Modeling of atmospheric chemistry*. Cambridge University Press. https://doi.org/10.1017/9781316544754

Brasseur, G., & Solomon, S. (1986). *Aeronomy of the middle atmosphere: Chemistry and physics of the stratosphere and mesosphere* (2nd ed.). D. Reidel. https://doi.org/10.1007/1-4020-3824-0

Broquet, A., & Andrews-Hanna, J. (2023). Geophysical evidence for an active mantle plume underneath Elysium Planitia on Mars. *Nature Astronomy*, *7*(2), 160–169. https://doi.org/10.1038/s41550-022-01836-3

Burkholder, J., Sander, S., Abbatt, J., Barker, J., Cappa, C., Crounse, J., et al. (2019). Chemical kinetics and photochemical data for use in atmospheric studies. Evaluation no. 19 (Tech. Rep. No. 19-5).

Campbell, I., & Gray, C. (1973). Rate constants for $O(^3P)$ recombination and association with $N(^4S)$. *Chemical Physics Letters*, *18*(4), 607–609. https://doi.org/10.1016/0009-2614(73)80479-8

Catling, D., Claire, M., Zahnle, K., Quinn, R., Clark, B., Hecht, M., & Kounaves, S. (2010). Atmospheric origins of perchlorate on Mars and in the Atacama. *Journal of Geophysical Research*, *115*(E1). https://doi.org/10.1029/2009JE003425

Cheng, B.-M., Chew, E., Liu, C.-P., Bahou, M., Lee, Y.-P., Yung, Y., & Gerstell, M. (1999). Photo-induced fractionation of water isotopomers in the Martian atmosphere. *Geophysical Research Letters*, *26*(24), 3657–3660. https://doi.org/10.1029/1999GL008367

Colaïtis, A., Spiga, A., Hourdin, F., Rio, C., Forget, F., & Millour, E. (2013). A thermal plume model for the Martian convective boundary layer. *Journal of Geophysical Research: Planets*, *118*(7), 1468–1487. https://doi.org/10.1002/jgre.20104

Edgar, J., Gould, J., Badreshany, K., & Telling, J. (2022). Mechanochemical generation of perchlorate. *Icarus*, *387*, 115202. https://doi.org/10.1016/j.icarus.2022.115202

Forget, F., Hourdin, F., Fournier, R., Hourdin, C., Talagrand, O., Collins, M., et al. (1999). Improved general circulation models of the Martian atmosphere from the surface to above 80 km. *Journal of Geophysical Research*, *104*(E10), 24155–24175. https://doi.org/10.1029/1999JE001025

Forget, F., Millour, E., Bierjon, A., Delavois, A., Fan, S., Lange, L., et al. (2022). Challenges in Mars climate modelling with the LMD Mars global climate model, now called the Mars "Planetary Climate Model" (PCM). In *Seventh international workshop on the mars atmosphere: Modelling and observations* (p. 1102).

Glavin, D., Freissinet, C., Miller, K., Eigenbrode, J., Brunner, A., Buch, A., et al. (2013). Evidence for perchlorates and the origin of chlorinated hydrocarbons detected by SAM at the Rocknest aeolian deposit in Gale Crater. *Journal of Geophysical Research: Planets*, *118*(10), 1955–1973. https://doi.org/10.1002/jgre.20144

Gough, R., Tolbert, M., McKay, C., & Toon, O. (2010). Methane adsorption on a Martian soil analog: An abiogenic explanation for methane variability in the Martian atmosphere. *Icarus*, *207*(1), 165–174. https://doi.org/10.1016/j.icarus.2009.11.030

Hartogh, P., Jarchow, C., Lellouch, E., de Val-Borro, M., Rengel, M., Moreno, R., et al. (2010). Herschel/HIFI observations of Mars: First detection of O2 at submillimetre wavelengths and upper limits on HCl and H2O2. *Astronomy and Astrophysics*, *521*, L49. https://doi.org/10.1051/0004-6361/201015160

Hauber, E., Brož, P., Jagert, F., Jodłowski, P., & Platz, T. (2011). Very recent and wide-spread basaltic volcanism on Mars. *Geophysical Research Letters*, *38*(10). https://doi.org/10.1029/2011GL047310

Hecht, M., Kounaves, S., Quinn, R., West, S., Young, S., Ming, D., et al. (2009). Detection of perchlorate and the soluble chemistry of Martian soil at the Phoenix lander site. *Science*, *325*(5936), 64–67. https://doi.org/10.1126/science.1172466

Holmes, J., Lewis, S., & Patel, M. (2020). Openmars: A global record of Martian weather from 1999 to 2015. *Planetary and Space Science*, *188*, 104962. https://doi.org/10.1016/j.pss.2020.104962

Holmes, J., Lewis, S., Patel, M., Alday, J., Aoki, S., Liuzzi, G., et al. (2022). Global variations in water vapor and saturation state throughout the Mars Year 34 dusty season. *Journal of Geophysical Research: Planets*, *127*(10), e2022JE007203. https://doi.org/10.1029/2022JE007203

Hoskins, B., & Simmons, A. (1975). A multi-layer spectral model and the semi-implicit method. *The Quarterly Journal of the Royal Meteorological Society*, *101*(429), 637–655. https://doi.org/10.1002/qj.49710142918

Keller, J., Boynton, W., Karunatillake, S., Baker, V., Dohm, J., Evans, L., et al. (2006). Equatorial and midlatitude distribution of chlorine measured by Mars Odyssey GRS. *Journal of Geophysical Research*, *111*(E3). https://doi.org/10.1029/2006JE002679

Kieffer, H., Martin, T., Peterfreund, A., Jakosky, B., Miner, E., & Palluconi, F. (1977). Thermal and albedo mapping of Mars during the Viking primary mission. *Journal of Geophysical Research*, *82*(28), 4249–4291. https://doi.org/10.1029/JS082i028p04249

Korablev, O., Olsen, K., Trokhimovskiy, A., Lefèvre, F., Montmessin, F., Fedorova, A., et al. (2021). Transient HCl in the atmosphere of Mars. *Science Advances*, *7*(7), eabe4386. https://doi.org/10.1126/sciadv.abe4386

Krasnopolsky, V. (2022). Photochemistry of HCl in the martian atmosphere. *Icarus*, *374*, 114807. https://doi.org/10.1016/j.icarus.2021.114807

Lefèvre, F., & Krasnopolsky, V. (2017). Atmospheric photochemistry. In R. Haberle, R. Clancy, F. Forget, M. Smith, & R. Zurek (Eds.), *The atmosphere and climate of mars* (pp. 405–432). Cambridge University Press. https://doi.org/10.1017/9781139060172.013

Lefèvre, F., Lebonnois, S., Montmessin, F., & Forget, F. (2004). Three-dimensional modeling of ozone on Mars. *Journal of Geophysical Research*, *109*(E7). https://doi.org/10.1029/2004JE002268

Lewis, B., & Carver, J. (1983). Temperature dependence of the carbon dioxide photoabsorption cross section between 1200 and 1970 Å. *Journal of Quantitative Spectroscopy and Radiative Transfer*, *30*(4), 297–309. https://doi.org/10.1016/0022-4073(83)90027-4

Lewis, S., & Barker, P. (2005). Atmospheric tides in a Mars general circulation model with data assimilation. *Advances in Space Research*, *36*(11), 2162–2168. https://doi.org/10.1016/j.asr.2005.05.122

Lorenc, A., Bell, R., & Macpherson, B. (1991). The Meteorological Office analysis correction data assimilation scheme. *The Quarterly Journal of the Royal Meteorological Society*, *117*(497), 59–89. https://doi.org/10.1002/qj.49711749704

Luginin, M., Trokhimovskiy, A., Taysum, B., Fedorova, A., Korablev, O., Olsen, K., et al. (2024). Evidence of rapid hydrogen chloride uptake on water ice in the atmosphere of Mars. *Icarus*, *411*, 115960. https://doi.org/10.1016/j.icarus.2024.115960

Madeleine, J., Forget, F., Millour, E., Montabone, L., & Wolff, M. (2011). Revisiting the radiative impact of dust on Mars using the LMD Global Climate Model. *Journal of Geophysical Research*, *116*(E11), E11010. https://doi.org/10.1029/2011JE003855

Madronich, S., & Flocke, S. (1999). The role of solar radiation in atmospheric chemistry. In P. Boule (Ed.), *Environmental photochemistry* (pp. 1–26). Cambridge University Press. https://doi.org/10.1007/978-3-540-69044-3_1

McKeachie, J., Appel, M., Kirchner, U., Schindler, R., & Benter, T. (2004). Observation of a heterogeneous source of OClO from the reaction of ClO radicals on ice. *Journal of Physical Chemistry B*, *108*(43), 16786–16797. https://doi.org/10.1021/jp049314p

Minschwaner, K., Anderson, G., Hall, L., & Yoshino, K. (1992). Polynomial coefficients for calculating O2 Schumann-Runge cross sections at 0.5 cm- 1 resolution. *Journal of Geophysical Research*, *97*(D9), 10103–10108. https://doi.org/10.1029/92JD00661

Montabone, L., Forget, F., Millour, E., Wilson, R., Lewis, S., Cantor, B., et al. (2015). Eight-year climatology of dust optical depth on Mars. *Icarus*, *251*, 65–95. https://doi.org/10.1016/j.icarus.2014.12.034

Montabone, L., Spiga, A., Kass, D., Kleinböhl, A., Forget, F., & Millour, E. (2020). Martian year 34 column dust climatology from Mars climate sounder observations: Reconstructed maps and model simulations. *Journal of Geophysical Research: Planets*, *125*(8), e2019JE006111. https://doi.org/10.1029/2019JE006111

Murchie, S., Mustard, J., Ehlmann, B., Milliken, R., Bishop, J., McKeown, N., et al. (2009). A synthesis of Martian aqueous mineralogy after 1 Mars year of observations from the Mars Reconnaissance Orbiter. *Journal of Geophysical Research*, *114*(E2). https://doi.org/10.1029/2009JE003342

Navarro, T., Madeleine, J.-B., Forget, F., Spiga, A., Millour, E., Montmessin, F., & Määttänen, A. (2014). Global climate modeling of the Martian water cycle with improved microphysics and radiatively active water ice clouds. *Journal of Geophysical Research: Planets*, *119*(7), 1479–1495. https://doi.org/10.1002/2013JE004550

Newman, C., Lewis, S., Read, P., & Forget, F. (2002). Modeling the Martian dust cycle, 1. Representations of dust transport processes. *Journal of Geophysical Research*, *107*(E12), 1–6. https://doi.org/10.1029/2002JE001910

Olsen, K., Fedorova, A., Kass, D., Kleinböhl, A., Trokhimivskiy, A., Korablev, O., et al. (2024a). Relationships between HCl, H2O, aerosols and temperature in the Martian atmosphere Part I: Climatological outlook. *Journal of Geophysical Research: Planets*, *129*(8), e2024JE008350. https://doi.org/10.1029/2024JE008350

Olsen, K., Fedorova, A., Kass, D., Kleinböhl, A., Trokhimivskiy, A., Korablev, O., et al. (2024b). Relationships between HCl, H2O, aerosols and temperature in the Martian atmosphere Part II: Quantitative correlations. *Journal of Geophysical Research: Planets*, *129*(8), e2024JE008351. https://doi.org/10.1029/2024JE008351

Olsen, K., Lefèvre, F., Montmessin, F., Fedorova, A., Trokhimovskiy, A., Baggio, L., et al. (2021). The vertical structure of CO in the Martian atmosphere from the ExoMars Trace Gas Orbiter. *Nature Geoscience*, *14*(2), 67–71. https://doi.org/10.1038/s41561-020-00678-w

Olsen, K., Trokhimovskiy, A., Montabone, L., Fedorova, A., Luginin, M., Lefèvre, F., et al. (2021). Seasonal reappearance of HCl in the atmosphere of Mars during the Mars year 35 dusty season. *Astronomy and Astrophysics*, *647*, A161. https://doi.org/10.1051/0004-6361/202140329

Osterloo, M., Hamilton, V., Bandfield, J., Glotch, T., Baldridge, A., Christensen, P., et al. (2008). Chloride-bearing materials in the southern highlands of Mars. *Science*, *319*(5870), 1651–1654. https://doi.org/10.1126/science.1150690

Papanastasiou, D., Papadimitriou, V., Fahey, D., & Burkholder, J. (2009). UV absorption spectrum of the ClO dimer (Cl2O2) between 200 and 420 nm. *Journal of Physical Chemistry A*, *113*(49), 13711–13726. https://doi.org/10.1021/jp9065345

Parkinson, W., Rufus, J., & Yoshino, K. (2003). Absolute absorption cross section measurements of CO2 in the wavelength region 163–200 nm and the temperature dependence. *Chemical Physics*, *290*(2–3), 251–256. https://doi.org/10.1016/S0301-0104(03)00146-0

Rajendran, K., Lewis, S., Holmes, J., Streeter, P., Fedorova, A., & Patel, M. (2021). Enhanced super-rotation before and during the 2018 Martian global dust storm. *Geophysical Research Letters*, *48*(16), e2021GL094634. https://doi.org/10.1029/2021GL094634

Rajendran, K., Streeter, P., Lewis, S., Patel, M., Duffy, M., Holmes, J., et al. (2024). A Martian global climate model with gas-phase chemistry, transport and surface deposition of chlorine species [Dataset]. *Open Research Data Online*. https://doi.org/10.21954/ou.rd.25848157

Ruesch, O., Poulet, F., Vincendon, M., Bibring, J.-P., Carter, J., Erkeling, G., et al. (2012). Compositional investigation of the proposed chloride-bearing materials on Mars using near-infrared orbital data from OMEGA/MEx. *Journal of Geophysical Research*, *117*(E11). https://doi.org/10.1029/2012JE004108

Ruf, C., Renno, N., Kok, J., Bandelier, E., Sander, M., Gross, S., et al. (2009). Emission of non-thermal microwave radiation by a Martian dust storm. *Geophysical Research Letters*, *36*(13). https://doi.org/10.1029/2009GL038715

Sander, S., Abbatt, J., Barker, J., Burkholder, J., Friedl, R., Golden, D., et al. (2011). Chemical kinetics and photochemical data for use in atmospheric studies. Evaluation no. 17 (Tech. Rep. No. 10-6).

Sander, S., Friedl, R., Golden, D., Kurylo, M., Huie, R., Orkin, V., et al. (2003). Chemical kinetics and photochemical data for use in atmospheric studies. Evaluation no. 14 (Tech. Rep. No. 02-25).

Sander, S., Friedl, R., Golden, D., Kurylo, M., Moortgat, G., Wine, P., et al. (2006). Chemical kinetics and photochemical data for use in atmospheric studies. Evaluation no. 15 (Tech. Rep. No. 06-2).

Schergers, M., & Welge, K. (1968). Absorption coefficient of H202 and N2H4 between 1200 and 2000 Å. *Zeitschrift für Naturforschung*, *A*(10), 1508.

Shimazaki, T. (1985). *Minor constituents in the middle atmosphere*. Springer.

Simmons, A., & Burridge, D. (1981). An energy and angular-momentum conserving vertical finite-difference scheme and hybrid vertical coordinates. *Monthly Weather Review*, *109*(4), 758–766. https://doi.org/10.1175/1520-0493(1981)109⟨0758:AEAAMC⟩2.0.CO;2

Simonaitis, R., & Heicklen, J. (1975). Perchloric acid: A possible sink for stratospheric chlorine. *Planetary and Space Science*, *23*(11), 1567–1569. https://doi.org/10.1016/0032-0633(75)90010-0

Smith, M., Claire, M., Catling, D., & Zahnle, K. (2014). The formation of sulfate, nitrate and perchlorate salts in the Martian atmosphere. *Icarus*, *231*, 51–64. https://doi.org/10.1016/j.icarus.2013.11.031

Solomon, S. (1999). Stratospheric ozone depletion: A review of concepts and history. *Review of Geophysics*, *37*(3), 275–316. https://doi.org/10.1029/1999RG900008

Streeter, P., Lewis, S., Patel, M., Holmes, J., Fedorova, A., Kass, D., & Kleinböhl, A. (2021). Asymmetric impacts on Mars' polar vortices from an equinoctial global dust storm. *Journal of Geophysical Research: Planets*, *126*(5), e2020JE006774. https://doi.org/10.1029/2020JE006774

Streeter, P., Lewis, S., Patel, M., Holmes, J., & Rajendran, K. (2023). An eight-year climatology of the Martian northern polar vortex. *Icarus*, *115864*, 115864. https://doi.org/10.1016/j.icarus.2023.115864

Streeter, P. M., Rajendran, K., Lewis, S. R., Olsen, K. S., Trokhimovskiy, A., Korablev, O., & Patel, M. R. (2025). Global distribution and seasonality of Martian atmospheric HCl explained through heterogeneous chemistry. *Geophysical Research Letters*, *52*, e2024GL111059. https://doi.org/10.1029/2024GL111059

Sullivan, R., Guazzotti, S., Sodeman, D., Tang, Y., Carmichael, G., & Prather, K. (2007). Mineral dust is a sink for chlorine in the marine boundary layer. *Atmospheric Environment*, *41*(34), 7166–7179. https://doi.org/10.1016/j.atmosenv.2007.05.047

Taysum, B., Palmer, P., Olsen, K., Luginin, M., Ignatiev, N., Trokhimovskiy, A., et al. (2024). Observed seasonal changes in Martian hydrogen chloride explained by heterogeneous chemistry. *Astronomy and Astrophysics*, *687*, A191. https://doi.org/10.1051/0004-6361/202449546

Trolier, M., Mauldin, R., & Ravishankara, A. (1990). Rate coefficient for the termolecular channel of the self-reaction of chlorine monoxide. *Journal of Physical Chemistry*, *94*(12), 4896–4907. https://doi.org/10.1021/j100375a027

Villanueva, G., Mumma, M., Novak, R., Radeva, Y., Käufl, H., Smette, A., et al. (2013). A sensitive search for organics (CH4, CH3OH, H2CO, C2H6, C2H2, C2H4), hydroperoxyl (HO2), nitrogen compounds (N2O, NH3, HCN) and chlorine species (HCl, CH3Cl) on Mars using ground-based high-resolution infrared spectroscopy. *Icarus*, *223*(1), 11–27. https://doi.org/10.1016/j.icarus.2012.11.013

Wahner, A., Tyndall, G., & Ravishankara, A. (1987). Absorption cross sections for symmetric chlorine dioxide as a function of temperature in the wavelength range 240-480 nm. *Journal of Physical Chemistry*, *91*(11), 2734–2738. https://doi.org/10.1021/j100295a018

Wilson, E., Atreya, S., Kaiser, R., & Mahaffy, P. (2016). Perchlorate formation on mars through surface radiolysis-initiated atmospheric chemistry: A potential mechanism. *Journal of Geophysical Research: Planets*, *121*(8), 1472–1487. https://doi.org/10.1002/2016JE005078

Wu, Z., Wang, A., Farrell, W., Yan, Y., Wang, K., Houghton, J., & Jackson, A. (2018). Forming perchlorates on Mars through plasma chemistry during dust events. *Earth and Planetary Science Letters*, *504*, 94–105. https://doi.org/10.1016/j.epsl.2018.08.040

Xu, Z., & Lin, M.-C. (2003). Ab initio studies of ClOx reactions. IX. Combination and disproportionation reactions of ClO and s-ClO3 radicals. *Journal of Chemical Physics*, *119*(17), 8897–8904. https://doi.org/10.1063/1.1613632

Yoshino, K., Cheung, A.-C., Esmond, J., Parkinson, W., Freeman, D., Guberman, S., et al. (1988). Improved absorption cross-sections of oxygen in the wavelength region 205–240 nm of the Herzberg continuum. *Planetary and Space Science*, *36*(12), 1469–1475. https://doi.org/10.1016/0032-0633(88)90012-8

Yoshino, K., Esmond, J., Parkinson, W., Ito, K., & Matsui, T. (1996). Absorption cross section measurements of water vapor in the wavelength region 120 to 188 nm. *Chemical Physics*, *211*(1–3), 387–391. https://doi.org/10.1016/0301-0104(96)00210-8

Yoshino, K., Esmond, J., Sun, Y., Parkinson, W., Ito, K., & Matsui, T. (1996). Absorption cross section measurements of carbon dioxide in the wavelength region 118.7–175.5 nm and the temperature dependence. *Journal of Quantitative Spectroscopy and Radiative Transfer*, *55*(1), 53–60. https://doi.org/10.1016/0022-4073(95)00135-2

Zhu, R., & Lin, M.-C. (2001). Ab initio study of ammonium perchlorate combustion initiation processes: Unimolecular decomposition of perchloric acid and the related OH + ClO3 reaction. *PhysChemComm*, *4*(25), 127–132. https://doi.org/10.1039/B109523B

Zhu, R., & Lin, M.-C. (2004). Ab initio studies of ClOx reactions: Prediction of the rate constants of ClO+NO for the forward and reverse processes. *ChemPhysChem*, *5*(12), 1864–1870. https://doi.org/10.1002/cphc.200400305